Nonlinear vibratory energy exchanges in a meta-cell

Camila da Silveira Zanin, Alireza Ture Savadkoohi, Sébastien Baguet, Régis Dufour, Gabriel Hurel

Nonlinear vibratory energy exchanges in a meta-cell

C. da Silveira Zanin[a,b,*], A. Ture Savadkoohi[a], S. Baguet[b], R. Dufour[b], G. Hurel[a,b]

[a] *Univ Lyon, ENTPE, LTDS UMR CNRS 5513, 69518 Vaulx-en-Velin, France*
[b] *Univ Lyon, INSA Lyon, LaMCoS UMR CNRS 5259, 69621 Villeurbanne, France*

Abstract

Meta-materials are utilized for bringing passive attenuation solution especially in the acoustics and vibration domains. Generally speaking, they are composed of an array or a chain of meta-cells. Here the vibratory energy exchanges between particles of a nonlinear meta-cell are studied. The meta-cell is composed of an outer mass which houses an inner mass with a compound nonlinear restoring forcing term. It is globally non-smooth, containing pure cubic and piece-wise linear terms, which constitutes a new type of nonlinearity for such mass-in-mass cells. The complexified form of system equations is treated by the multiple time scale method to find out its fast and slow dynamics, leading to determination of the slow invariant manifold as well as the singular and equilibrium points of the system. The compound nonlinear restoring forcing function of the inner mass makes the global geometry of the slow invariant manifold to be different from those of systems with pure cubic nonlinearities, for example, including four singular lines and two distinct unstable zones. Amplitude dependency of the frequency of such a nonlinear system in the conservative form is represented by the backbone curves. Furthermore, detected equilibrium points for different external forcing amplitudes are represented by three-dimensional frequency response curves. Finally, analytical predictions are confronted with numerical results obtained by direct time integration of the system equations. An application of such system can be the passive control of main systems via embedding another nonlinear oscillator inside it. Moreover, such system can also be extended in the form of an array to create meta-materials.

Keywords: meta-cell, nonlinear restoring force, slow invariant manifold, equilibrium/singular points, isola

1. Introduction

The passive vibratory energy control of different types of systems demands exploitation of linear or nonlinear nature of some other coupled oscillators. The well established linear system is named as Frahm device [1] or tuned mass damper [2]. Such linear devices are very efficient around the tuned frequency, however they lose their efficiencies elsewhere. To overcome this drawback, Roberson [3] supplemented a cubic part to the linear restoring forcing function of the vibration absorber showing that its range of working frequency increases with respect to the linear absorber. Then, the work of Roberson was extended by Henry and Tobias [4, 5] to consider a general model of two degrees of freedom (dof) nonlinear systems focusing on endowing nonlinear characteristics of coupled oscillators for control and isolation. Since then, different types of nonlinear passive absorbers have been developed: pendulum type [6, 7], autoparametric [8], magnetic field based nonlinear absorbers [9, 10], nonlinear softening controllers via arrays of Belleville washers mounted back to back [11, 12], the bow-type or shallow springs (or shallow buckled beam) [13], impact dampers [14, 15] and nonlinear energy sink (NES) [16, 17, 18]. The NES in its early developments was composed of a cubic nonlinear restoring forcing function [17]. Then, other types of nonlinearaties were exploited for designing the NES: i) nonsmooth systems including vibro impact [19, 20, 21], piece-wise linear [22, 23, 24] and Bouc-Wen type [25]. Such systems have been applied in many domains such as mechanics and acoustics, with applications in aeroelastic domains [26, 27, 28, 29, 30], structural engineering [31, 32, 33] and noise control [34, 35]. In this paper, we consider a grounded cell composed of an outer mass which houses an inner mass. The coupling between the two masses is a spacial combinational nonlinearity. The global form of governing system equations are

*Corresponding author - camila.zanin@entpe.fr

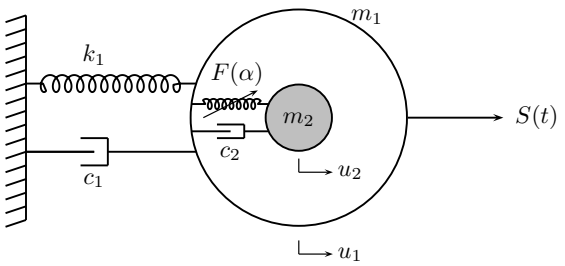

Figure 1: Model of the mass-in-mass meta-cell. The inner mass, m_2, with nonlinear restoring forcing function $F(\alpha)$ is housed by the outer mass m_1.

.

the same as two coupled oscillators, such as a main system and a NES. In this paper, we aim to develop analytical tools for designing this system, which can be used for the passive control of the outer mass or as a first step towards an array of nonlinear mass-in-mass meta-cells. Such systems can present interesting properties such as negative equivalent mass and stiffness [36].

This paper is organized as follows: The studied system is presented in Sect. 2. Analytical methods applied for solving the equations of motion are discussed in Sect. 3. Different system dynamics are detected in Sect. 4. Analytical results are compared with numerical ones in Sect. 5. Finally, conclusions are drawn in Sect. 6.

2. The mass-in-mass cell model

The mass-in-mass cell unit considered in this paper is shown in Fig. 1. It consists of an outer rigid mass m_1 with generalized displacement u_1 and an inner rigid mass m_2 having the generalized displacement u_2. The outer mass is grounded by a linear spring with constant stiffness k_1 and linear damping with a constant coefficient c_1. Both masses are coupled via a damping coefficient, c_2, and a nonlinear restoring force, $F(\alpha)$, function of the relative displacement of the two masses. Besides that, the primary system is forced by an external sinusoidal excitation $S(t) = P\sin(\Omega t)$.

The governing system equations in the time domain t are:

$$\begin{cases} m_1 u_1'' + k_1 u_1 + c_1 u_1' + F(u_1 - u_2) + c_2(u_1' - u_2') = P\sin(\Omega t) \\ m_2 u_2'' + F(u_2 - u_1) + c_2(u_2' - u_1') = 0 \end{cases} \tag{1}$$

where $(.)'$ stands for derivative with respect to t.

Let us suppose that $F(\alpha)$ is odd, reading as:

$$F(\alpha) = -F(-\alpha) = \begin{cases} k_{NL}\alpha^3 & \text{if} \quad -\delta \le \alpha \le \delta \\ k_L(\alpha - \delta) + k_{NL}\delta^3 & \text{if} \quad \alpha > \delta \\ k_L(\alpha + \delta) - k_{NL}\delta^3 & \text{if} \quad \alpha < -\delta \end{cases} \tag{2}$$

In details, the function $F(\alpha)$ is cubic in the clearance of 2δ and it becomes linear elsewhere. The schematic representation of $F(\alpha)$ is illustrated in Fig. 2. Let us introduce a nondimensionalized time τ as:

$$\tau = \omega t = \sqrt{\frac{k_1}{m_1}}t \tag{3}$$

We assume $0 < \epsilon = \frac{m_2}{m_1} \ll 1$ and the following parameters are introduced:

$$\begin{aligned} &\epsilon\zeta_1 = \frac{c_1}{\sqrt{k_1 m_1}}, \epsilon\zeta_2 = \frac{c_2}{\sqrt{k_1 m_1}}, \epsilon\gamma = \frac{P}{k_1}, = \frac{\Omega}{\omega} \\ &\epsilon f(u_1 - u_2) = \frac{F(u_1 - u_2)}{k_1}, \epsilon K_{NL} = \frac{k_{NL}}{k_1}, \epsilon K_L = \frac{k_L}{k_1} \end{aligned} \tag{4}$$

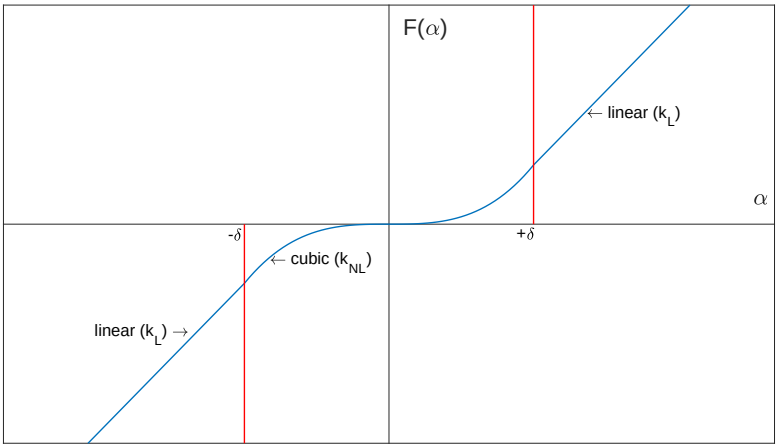

Figure 2: The odd restoring forcing function $F(\alpha)$ (see Eq. (2)).

Consequently, Eq. (1) adopts the dimensionless expression:

$$\begin{cases} \ddot{u}_1 + u_1 + \epsilon\zeta_1\dot{u}_1 + \epsilon f(u_1 - u_2) + \epsilon\zeta_2(\dot{u}_1 - \dot{u}_2) = \epsilon\gamma\sin(\vartheta\tau) \\ \epsilon\ddot{u}_2 + \epsilon f(u_2 - u_1) + \epsilon\zeta_2(\dot{u}_2 - \dot{u}_1) = 0 \end{cases} \tag{5}$$

where $(\dot{\ })$ stands for the derivative with respect to τ.
Moreover, we introduce new variables w and v which correspond to the centre of mass of the two particles and the relative displacement, respectively:

$$\begin{bmatrix} w \\ v \end{bmatrix} = \begin{bmatrix} 1 & \epsilon \\ 1 & -1 \end{bmatrix} \begin{bmatrix} u_1 \\ u_2 \end{bmatrix} \tag{6}$$

Then Eq. (5) can be re-written in the following form:

$$\begin{cases} \ddot{w} + w + \epsilon v + \epsilon\zeta_1(\dot{w} + \epsilon\dot{v}) = \epsilon\gamma\sin(\vartheta\tau) \\ \ddot{v} + w + \epsilon v + \epsilon\zeta_1(\dot{w} + \epsilon\dot{v}) + f(v)(\epsilon + 1) + \zeta_2\dot{v}(\epsilon + 1) = \epsilon\gamma\sin(\vartheta\tau) \end{cases} \tag{7}$$

In the next section, the system variables will be complexified and a Galerkin method will be applied to system equations.

3. Complexification and multiple time scales method

The complex variables of Manevitch [37, 38] are applied according to the following relationship:

$$\begin{cases} \varphi_1 e^{i\vartheta\tau} = \dot{w} + i\vartheta w \\ \varphi_2 e^{i\vartheta\tau} = \dot{v} + i\vartheta v \end{cases} \tag{8}$$

with $i^2 = -1$.
According to the multiple time scales method [39], the time is decomposed in fast (τ_0) and slow scales ($\tau_j = \epsilon^j\tau$, $j = 1, 2, ...$). Then, we can write:

$$\frac{\mathrm{d}}{\mathrm{d}\tau} = \frac{\partial}{\partial\tau_0} + \epsilon\frac{\partial}{\partial\tau_1} + ... \tag{9}$$

A Galerkin method based on the truncated Fourier series, via keeping the first harmonics of the system, is used. For a generic function $H(\varphi_1, \varphi_2, \varphi_1^*, \varphi_2^*)$, this task is accomplished by:

$$X(\varphi_1, \varphi_2, \varphi_1^*, \varphi_2^*) = \frac{\vartheta}{2\pi} \int_0^{\frac{2\pi}{\vartheta}} H(\varphi_1, \varphi_2, \varphi_1^*, \varphi_2^*) e^{-i\vartheta\tau} d\tau \tag{10}$$

where $(.)^*$ stands for complex conjugate of a variable. It is assumed that $\varphi_1, \varphi_2, \varphi_1^*, \varphi_2^*$ do not depend on fast timescale, i.e., $\tau_0 = \tau$. The validity of this assumption will be checked during the multiple scale analysis or via searching an asymptotic state when $\tau_0 \to \infty$ [40].
Applying Eq. (8) and (10) in system (7), yields:

$$\begin{cases} \frac{1}{2}\dot{\varphi}_1 + \frac{i\vartheta\varphi_1}{2} + \frac{\varphi_1}{2i\vartheta} + \epsilon\zeta_1\left(\frac{\varphi_1}{2} + \epsilon\frac{\varphi_2}{2}\right) + \epsilon\frac{\varphi_2}{2i\vartheta} - \frac{\epsilon\gamma}{2i} = 0 \\ \\ \frac{1}{2}\dot{\varphi}_2 + \frac{i\vartheta}{2}\varphi_2 + \frac{\varphi_1}{2i\vartheta} + \epsilon\frac{\varphi_2}{2i\vartheta} + \epsilon\zeta_1\left(\frac{\varphi_1}{2} + \epsilon\frac{\varphi_2}{2}\right) + \mathcal{F}(\varphi_2, \varphi_2^*)(\epsilon + 1) + \zeta_2\frac{\varphi_2}{2}(\epsilon + 1) - \frac{\epsilon\gamma}{2i} = 0 \end{cases} \tag{11}$$

Where $\mathcal{F}(\varphi_2, \varphi_2^*)$ is:

$$\mathcal{F}(\varphi_2, \varphi_2^*) = \frac{\vartheta}{2\pi}\int_0^{\frac{2\pi}{\vartheta}} f\left(\frac{\varphi_2 e^{i\vartheta\tau} - \varphi_2^* e^{-i\vartheta\tau}}{2i\vartheta}\right) e^{-i\vartheta\tau} d\tau \tag{12}$$

It can be shown that

$$\mathcal{F}(\varphi_2, \varphi_2^*) = -\frac{i\varphi_2}{2\vartheta} G(|\varphi_2|^2), \tag{13}$$

where

$$G(|\varphi_2|^2) = \begin{cases} \frac{3K_{NL}|\varphi_2|^2}{4\vartheta^3} & \text{if } \frac{|\varphi_2|}{\vartheta} < \delta \\ \\ \frac{3K_{NL}|\varphi_2|^2}{4\vartheta^3} + \frac{1}{4\pi\vartheta^3|\varphi_2|}\left[\left(-8\delta K_L\vartheta^3\sqrt{1 - \frac{\delta^2\vartheta^2}{|\varphi_2|^2}}\right)\right. & \\ +K_{NL}\left(-6\delta|\varphi_2|^2\vartheta\sqrt{1 - \frac{\delta^2\vartheta^2}{|\varphi_2|^2}} + 12\delta^3\vartheta^3\sqrt{1 - \frac{\delta^2\vartheta^2}{|\varphi_2|^2}}\right) & \\ \left.+(8K_L|\varphi_2|\vartheta^2 - 6K_{NL}|\varphi_2|^3)\arccos\left(\frac{\delta\vartheta}{|\varphi_2|}\right)\right] & \text{if } \frac{|\varphi_2|}{\vartheta} \geq \delta \end{cases} \tag{14}$$

So one can write:

$$G(|\varphi_2|^2) = g(|\varphi_2|^2) + O(\epsilon^1) \tag{15}$$

where

$$g(|\varphi_2|^2) = \begin{cases} \frac{3K_{NL}|\varphi_2|^2}{4} & \text{if } |\varphi_2| < \delta \\ \\ \frac{3K_{NL}|\varphi_2|^2}{4} + \frac{1}{4\pi|\varphi_2|}\left[\left(-8\delta K_L\sqrt{1 - \frac{\delta^2}{|\varphi_2|^2}}\right)\right. & \\ +K_{NL}\left(-6\delta|\varphi_2|^2\sqrt{1 - \frac{\delta^2}{|\varphi_2|^2}} + 12\delta^3\sqrt{1 - \frac{\delta^2}{|\varphi_2|^2}}\right) & \\ \left.+(8K_L|\varphi_2| - 6K_{NL}|\varphi_2|^3)\arccos\left(\frac{\delta}{|\varphi_2|}\right)\right] & \text{if } |\varphi_2| \geq \delta \end{cases} \tag{16}$$

In the next section, Eq. (11) will be treated by the method of multiple scales [39] via looking at equations of different orders of ϵ. This will lead to the determination of different system dynamics, i.e., fast and slow ones [41]. It should be mentioned that there are other methods to detect dynamics of such coupled nonlinear systems, such as the harmonic balance method [42] which seeks for periodic regimes of the system.

ζ_1	ζ_2	γ
0.1	0.1	0

Table 1: Parameters of the system.

K_{NL}	K_L	δ
0.1	0.1	5

Table 2: Parameters of the nonlinear restoring forcing function.

4. Detection of different dynamics

4.1. Fast dynamics: ϵ^0 order of system equations

For ϵ^0 order, expansion (11) yields:

$$\begin{cases} \dfrac{\partial \varphi_1}{\partial \tau_0} = 0 \Rightarrow \varphi_1 = \varphi_1(\tau_1, \tau_2, ...) \\ \dfrac{\partial \varphi_2}{\partial \tau_0} = \mathscr{H}(\varphi_1, \varphi_2, \varphi_1^*, \varphi_2^*) \end{cases} \tag{17}$$

Let us seek for an asymptotic state of system when $\tau_0 \to \infty$. Therefore, it is assumed that when $\tau_0 \to \infty$, $\frac{\partial \varphi_2}{\partial \tau_0} \to 0$. Considering the system behaviours around a 1:1 resonance, setting $\vartheta = 1 + \sigma\epsilon$, where σ is a detuning parameter, Eq. (17) becomes:

$$\mathscr{H} = -i\varphi_2 + i\varphi_1 + i\varphi_2 g(|\varphi_2|^2) - \zeta_2\varphi_2 = 0 \tag{18}$$

$\mathscr{H}$ is called Slow Invariant Manifold (SIM), which is a geometrical representation for asymptotic states covering all equilibria of the system. It is worthwhile to mention that, looking to Eq. (17) and (18), the hypothesis of applying Eq. (10) is verified.

Let us express the complex variables of Manevitch in the polar domain as functions of amplitudes (N_j) and phases (δ_j):

$$\varphi_j = N_j e^{i\delta_j} \tag{19}$$

Where $N_j \in \mathbb{R}_+$ and $\delta_j \in \mathbb{R}$, $j = 1, 2$.

The SIM in real domain is obtained by applying Eq. (19) in (18). It reads:

$$N_1 = N_2 \sqrt{(1 - g(N_2^2))^2 + \zeta_2^2} \tag{20}$$

4.1.1. An example of SIM

Let us consider the parameters of Tables 1 and 2. The SIM of the system, obtained from Eq. (20), is presented in Fig. 3. It is seen that, considering a compound nonlinearity for the inner mass (see Eq. (2) and Fig. 2), the geometry of the SIM differs from corresponding ones of systems with pure cubic and piecewise-linear nonlinearities [43, 44], which present two local extrema, while here the SIM exhibits four local extrema.

4.2. Stability analysis of the SIM

In order to detect the stable areas of the SIM, the second equation of system (17) is linearized after linear perturbation of φ_2, as it follows:

$$\begin{cases} \varphi_2 \to \varphi_2 + \Delta\varphi_2 \\ \varphi_2^* \to \varphi_2^* + \Delta\varphi_2^* \end{cases} \tag{21}$$

where $|\Delta\varphi_2| << |\varphi_2|$.

Since φ_1 is independent of τ_0 (see the first equation of system (17)), we do not perturb φ_1 for this analysis. Applying

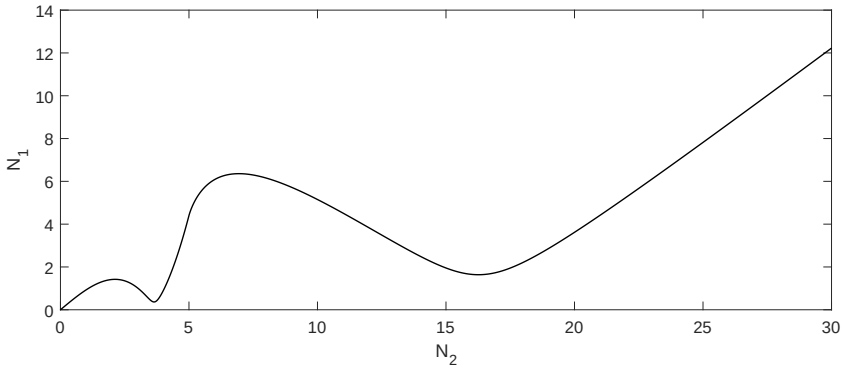

Figure 3: The SIM obtained from Eq. (20). Parameters of the system are reported in Tables 1 and 2.

the perturbed complex variables of Eq. (21) in Eq. (17), the following system can be obtained:

$$\begin{bmatrix} \dfrac{\partial \varphi_2}{\partial \tau_0} \\ \dfrac{\partial \varphi_2^*}{\partial \tau_0} \end{bmatrix} = \mathbf{M} \begin{bmatrix} \Delta\varphi_2 \\ \Delta\varphi_2^* \end{bmatrix} \tag{22}$$

with

$$\mathbf{M} = \begin{bmatrix} M_{11} & M_{12} \\ M_{21} & M_{22} \end{bmatrix} \tag{23}$$

The components of $\mathbf{M}$ are:

$$\begin{aligned} M_{11} &= i[g'(|\varphi_2|^2)|\varphi_2|^2 + g(|\varphi_2|^2) - 1] - \zeta_2 \\ M_{12} &= i\varphi_2^2 g'(|\varphi_2|^2) \\ M_{21} &= -i\varphi_2^{*2} g'(|\varphi_2|^2) \\ M_{22} &= -i[g'(|\varphi_2|^2)|\varphi_2|^2 + g(|\varphi_2|^2) - 1] - \zeta_2 \end{aligned}$$

where $g'(|\varphi_2|^2)$ is the derivative of Eq. (16) with respect to $|\varphi_2|^2$.
The characteristic equation of the matrix $\mathbf{M}$ is:

$$\det(\mathbf{M}) = \lambda^2 - (M_{11} + M_{22})\lambda + M_{11}M_{22} - M_{12}M_{21} = 0 \tag{24}$$

where λ_j, $j = 1, 2$, are eigenvalues of the system. The following relations can be defined from Eq. (24):

$$\begin{aligned} \lambda_1 + \lambda_2 &= M_{11} + M_{22} = -2\zeta_2 < 0 \\ \lambda_1\lambda_2 &= M_{11}M_{22} - M_{12}M_{21} \end{aligned} \tag{25}$$

We distinguish two cases:

- If $M_{11}M_{22} - M_{12}M_{21} > 0$:
  If λ_1 and λ_2 are real, then they both are certainly negative ($\lambda_1 + \lambda_2 < 0$), so the zone is stable;
  If λ_1 and λ_2 are complex, then their real parts should be $-\zeta_2$, so the zone is stable.
- If $M_{11}M_{22} - M_{12}M_{21} < 0$, then the real part of one of eigenvalues is positive, so the zone is unstable.

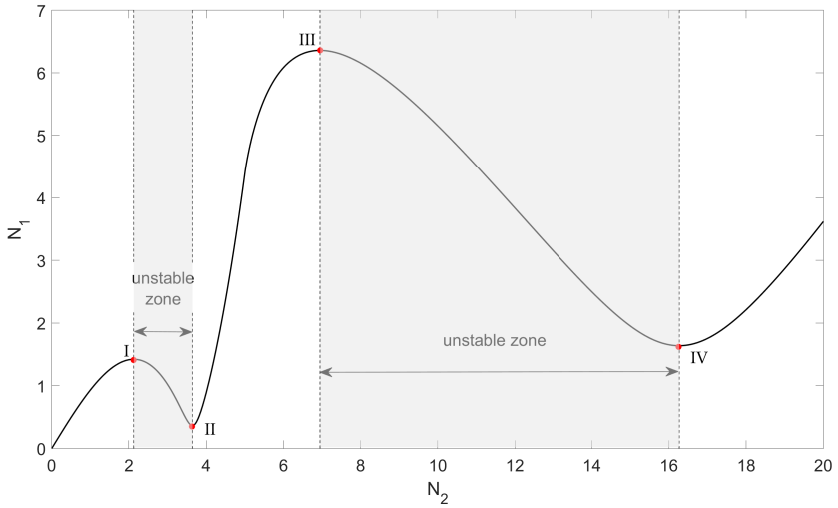

Figure 4: The SIM and its stability borders (- - -). Parameters of the system are reported in Tables 1 and 2.

As a summary, the borders between stable and unstable zones of the SIM can be written as:

$$M_{11}M_{22} - M_{12}M_{21} = 0 \tag{26}$$

which leads to:

$$1 - 2g(|\varphi_2|^2) + g^2(|\varphi_2|^2) - 2g'(|\varphi_2|^2)|\varphi_2|^2 + 2g(|\varphi_2|^2)g'(|\varphi_2|^2)|\varphi_2|^2 + g'^2(|\varphi_2|^2)|\varphi_2|^4 - g'^2(|\varphi_2|^2)\varphi_2^2\varphi_2^{*2} + \zeta_2^2 = 0 \tag{27}$$

Figure 4 collects the stability borders obtained by Eq. (27).

4.3. Slow dynamics: ϵ^1 order of system equations

The first equation of system (11) at $O(\epsilon^1)$ reads:

$$\frac{\mathrm{d}\varphi_1}{\mathrm{d}\tau_1} = E_1(\varphi_1, \varphi_2, \varphi_1^*, \varphi_2^*) \tag{28}$$

where

$$E_1(\varphi_1, \varphi_2, \varphi_1^*, \varphi_2^*) = -2i\sigma\varphi_1 - \zeta_1\varphi_1 + i\varphi_2 - i\gamma = 0 \tag{29}$$

The evolution of the SIM (see Eq. (18)) in τ_1 time scale leads to:

$$\begin{cases} \dfrac{\mathrm{d}\mathscr{H}}{\mathrm{d}\tau_1} = \dfrac{\partial\mathscr{H}}{\partial\varphi_1}\dfrac{\partial\varphi_1}{\partial\tau_1} + \dfrac{\partial\mathscr{H}}{\partial\varphi_1^*}\dfrac{\partial\varphi_1^*}{\partial\tau_1} + \dfrac{\partial\mathscr{H}}{\partial\varphi_2}\dfrac{\partial\varphi_2}{\partial\tau_1} + \dfrac{\partial\mathscr{H}}{\partial\varphi_2^*}\dfrac{\partial\varphi_2^*}{\partial\tau_1} = 0 \\ \dfrac{\mathrm{d}\mathscr{H}^*}{\mathrm{d}\tau_1} = \dfrac{\partial\mathscr{H}^*}{\partial\varphi_1}\dfrac{\partial\varphi_1}{\partial\tau_1} + \dfrac{\partial\mathscr{H}^*}{\partial\varphi_1^*}\dfrac{\partial\varphi_1^*}{\partial\tau_1} + \dfrac{\partial\mathscr{H}^*}{\partial\varphi_2}\dfrac{\partial\varphi_2}{\partial\tau_1} + \dfrac{\partial\mathscr{H}^*}{\partial\varphi_2^*}\dfrac{\partial\varphi_2^*}{\partial\tau_1} = 0 \end{cases} \tag{30}$$

Equation (30) can also be written in matrix form as:

$$\underbrace{\begin{bmatrix} \dfrac{\partial\mathscr{H}}{\partial\varphi_2} & \dfrac{\partial\mathscr{H}}{\partial\varphi_2^*} \\ \dfrac{\partial\mathscr{H}^*}{\partial\varphi_2} & \dfrac{\partial\mathscr{H}^*}{\partial\varphi_2^*} \end{bmatrix}}_{B} \begin{bmatrix} \dfrac{\partial\varphi_2}{\partial\tau_1} \\ \dfrac{\partial\varphi_2^*}{\partial\tau_1} \end{bmatrix} = - \begin{bmatrix} \dfrac{\partial\mathscr{H}}{\partial\varphi_1} & \dfrac{\partial\mathscr{H}}{\partial\varphi_1^*} \\ \dfrac{\partial\mathscr{H}^*}{\partial\varphi_1} & \dfrac{\partial\mathscr{H}^*}{\partial\varphi_1^*} \end{bmatrix} \begin{bmatrix} \dfrac{\partial\varphi_1}{\partial\tau_1} \\ \dfrac{\partial\varphi_1^*}{\partial\tau_1} \end{bmatrix} \tag{31}$$

Let us seek for singular and equilibrium points, which mainly correspond to non-periodic and periodic regimes, respectively [40]:

Singular points. The following conditions are set:

$$\begin{cases} E_1(\varphi_1, \varphi_2, \varphi_1^*, \varphi_2^*) = 0 \\ \mathscr{H}(\varphi_1, \varphi_2, \varphi_1^*, \varphi_2^*) = 0 \\ \det(B) = 0 \end{cases} \tag{32}$$

Equilibrium points. The following conditions are set:

$$\begin{cases} E_1(\varphi_1, \varphi_2, \varphi_1^*, \varphi_2^*) = 0 \\ \mathscr{H}(\varphi_1, \varphi_2, \varphi_1^*, \varphi_2^*) = 0 \\ \det(B) \neq 0 \end{cases} \tag{33}$$

It should be mentioned that if the singularities coincide with equilibrium points (i.e. fold singularities), the system repeatedly bifurcates, presenting strongly modulated responses [45].
From $\det(B) = 0$, the amplitudes of all possible singular points are determined as:

$$1 + g^2(N_2^2) - 2g(N_2^2) - 2N_2^2 g'(N_2^2) + 2N_2^2 g(N_2^2) g'(N_2^2) + \zeta_2^2 = 0 \tag{34}$$

Furthermore, when we solve $\frac{\partial N_1^2}{\partial N_2} = 0$ from Eq. (20) in order to find the local extrema of the SIM, we arrive at Eq. (34). This means that the positions of the singular points amplitudes, namely singular lines, coincide with those of local extrema of the SIM which are housed by stability borders as well. These extrema are marked as I, II, III and IV in Fig. 4.
From (33), equilibrium points are computed as:

$$\begin{aligned} &N_2^2 g^2(N_2^2)(4\sigma^2 + \zeta_1^2) + N_2^2 g(N_2^2)(-8\sigma^2 + 4\sigma - 2\zeta_1^2) \\ &+N_2^2(\zeta_1^2\zeta_2^2 + 2\zeta_1\zeta_2 + 4\sigma^2 - 4\sigma + 1 + \zeta_1^2 + 4\sigma^2\zeta_2^2) - \gamma^2 = 0 \end{aligned} \tag{35}$$

Detection of N_2 as roots of Eq. (35) in a direct manner is a challenging task due to the nature of the equation. If we reorganize this equation with respect to σ, it becomes a polynomial of degree two (Eq. (36)) which is easy to be solved.

$$\begin{aligned} &\left(4N_2^2 g^2(N_2^2) - 8N_2^2 g(N_2^2) + 4N_2^2 + 4N_2^2\zeta_2^2\right)\sigma^2 + \left(4N_2^2 g(N_2^2) - 4N_2^2\right)\sigma \\ &+N_2^2\left(g^2(N_2^2)\zeta_1^2 - 2g(N_2^2)\zeta_1^2 + \zeta_1^2\zeta_2^2 + 2\zeta_1\zeta_2 + 1 + \zeta_1^2\right) - \gamma^2 = 0 \end{aligned} \tag{36}$$

For a given N_2, Eq. (36) can be solved with respect to σ, then one can obtain the frequency response curve in term of N_2 for a given forcing amplitude γ. Subsequently, the frequency response curve in term of N_1 can be obtained by the equation of the SIM (see Eq. (20)).

4.4. Tracing the backbone curves of the system

After detection of all equilibrium points of the system, which are clarified in Eq. (36), we can obtain the backbone curves [39] via setting the excitation and damping terms of the system equals to zero. In other words, the backbone curves define nonlinear modal characteristics of conservative systems, showing an amplitude dependency of the frequency in the studied nonlinear system. The latter is a classical phenomenon in nonlinear dynamical systems. Thus, Eq. (36) reads:

$$\left(4g^2(N_2^2) - 8g(N_2^2) + 4\right)\sigma + 4g(N_2^2) - 4 = 0 \tag{37}$$

Backbone curves of the system as a function of detuning parameter σ or the frequency ($\vartheta = 1 + \sigma\epsilon$) are obtained from Eq. (37) and then from Eq. (20). The three-dimensional view of the backbone curves, which are composed of three branches, namely B1, B2 and B3, is illustrated in Fig. 5. The projection of Fig. 5 on the N_1-N_2 plane is plotted in Fig. 6, which represents the SIM of the system when damping terms are zero. These figures show the emergence of complicated and possibly non-continuous frequency responses, indicating the possible existence and positions of isola in the system. The frequency response curves of the meta-cell are presented in Sect. 5.2, followed by some more discussions on backbone curves in Sect. 5.3.

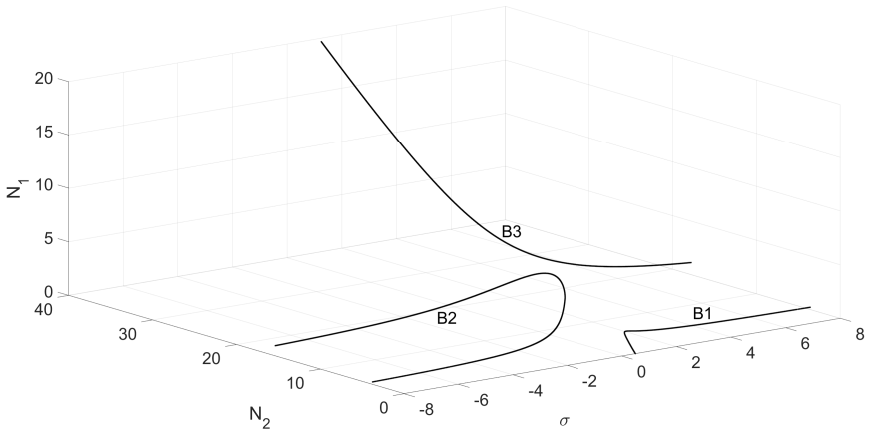

Figure 5: Backbone curves of the system.

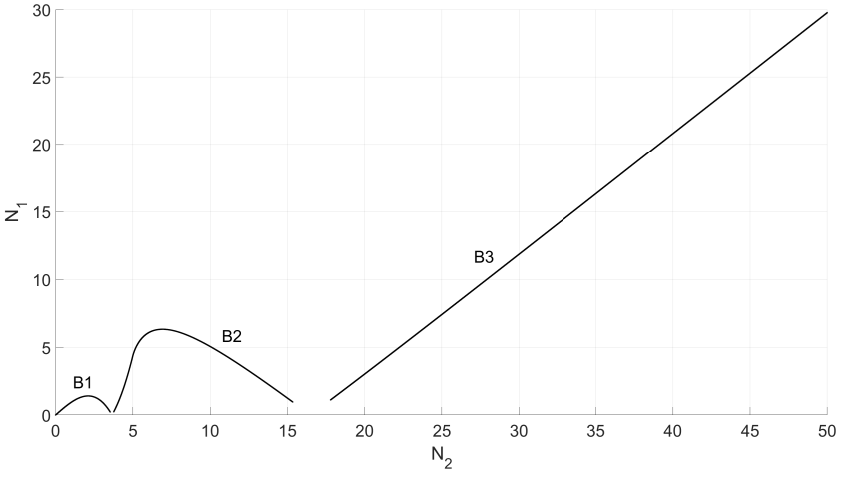

Figure 6: Projection of the backbone curves of Fig. 5 in the N1-N2 plane.

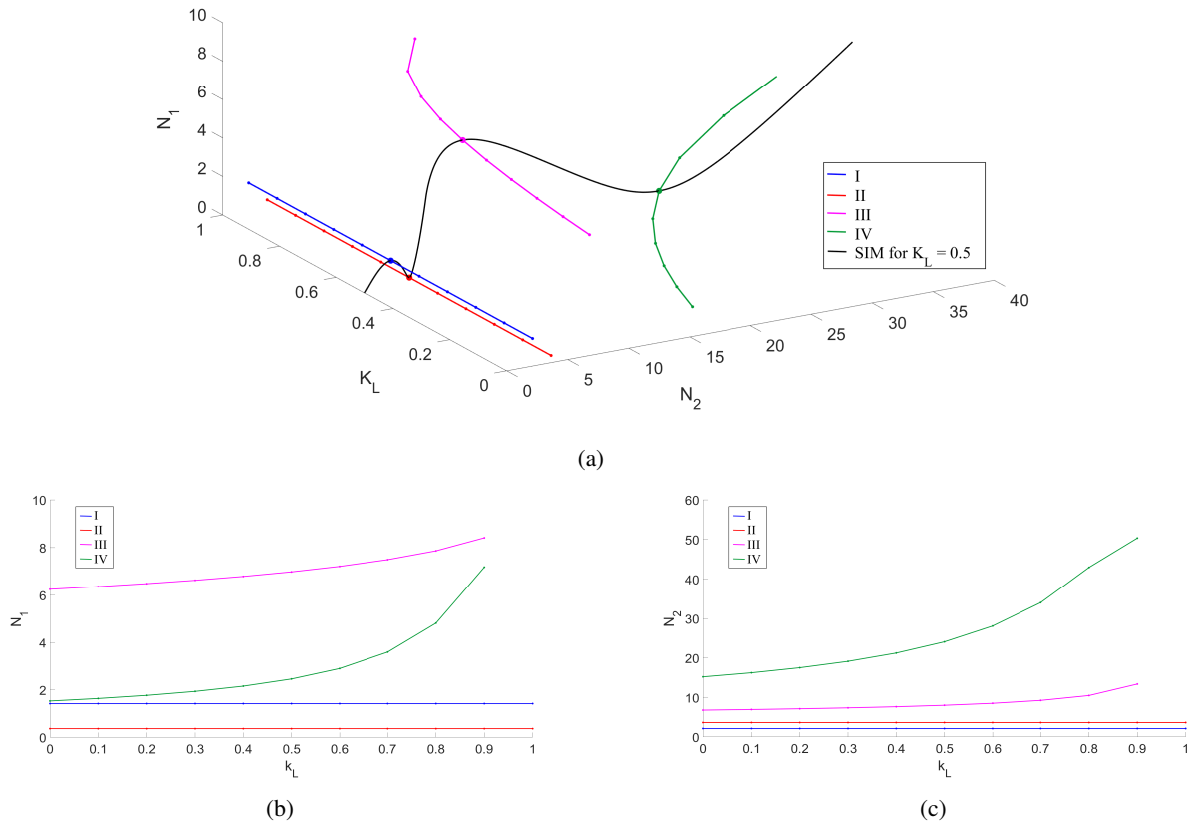

Figure 7: a) Amplitudes of singular points with respect to the parameter K_L of restoring forcing function. The black solid line represents the SIM of the system for $K_L = 0.5$ and the two other parameters of Table 2; b) N_1 versus K_L; c) N_2 versus K_L.

4.5. Fine tuning of the SIM via parametric study of the singular points

From Eq. (34), it is seen that the positions of singular lines depend on parameters of the non-linear restoring forcing function, which are provided in Table 2. In this subsection, the progressions of the singular lines are illustrated by varying each parameter of the restoring forcing function, i.e., K_L, K_{NL} and δ. In all figures presented here, the position of singular lines I and III (local maxima of the SIM) are in black and pink colour, respectively, while the position of II and IV (local minima of the SIM) are in red and green, respectively.

As an example, the three-dimensional view of positions of amplitudes of singular points, N_1 and N_2, for sweeping K_L and fixed two other parameters of Table 2 is illustrated in Fig. 7a. For the sake of clarity, a SIM is plotted in the same figure for $K_L = 0.5$. Two-dimensional views of this figure are presented in Figs. 7b and 7c. From these figures, it is noticed that K_L affects only the position of the singular lines III and IV of Fig. 4: if the value of K_L increases, their amplitudes in terms of N_1 and N_2 increase too. However, there is a value of K_L beyond which the singular lines III and IV do not exist. As an example, the corresponding SIM for $K_L = 1$ and other fixed parameters (see Table 2) is presented in Fig. 8, attesting the disappearance of local extrema III and IV.

For sweeping K_{NL}, the three-dimensional view of singular points amplitudes is illustrated in Fig. 9a and a SIM is plotted on the same figure for $K_{NL} = 0.5$. Two-dimensional views of Fig. 9a are presented in Figs. 9b and 9c. From these figures, it is seen that K_{NL} has influence on the position of all singular lines, but its effects are significant over the last two, namely on N_1 of the singular line III and on N_2 of IV.

For sweeping parameter δ, the three-dimensional view of the singular points amplitudes is illustrated in Fig. 10a. For

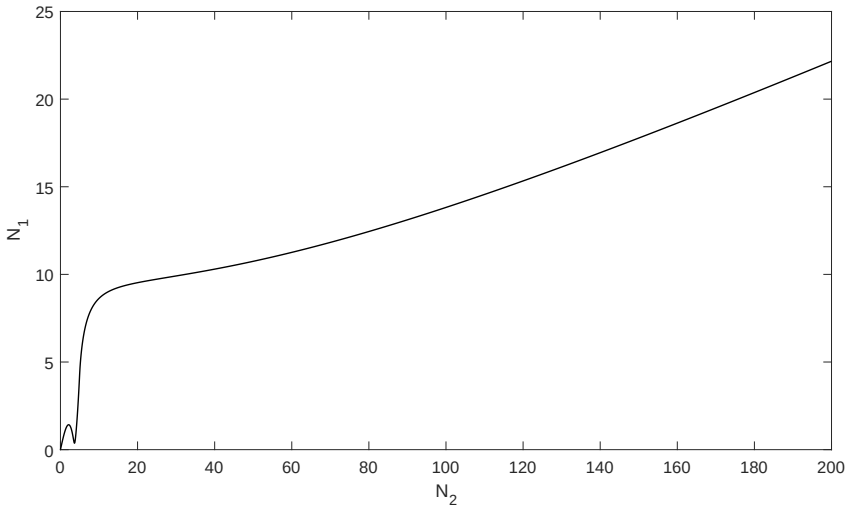

Figure 8: SIM for $K_L = 1$ and other fixed parameters of Table 2.

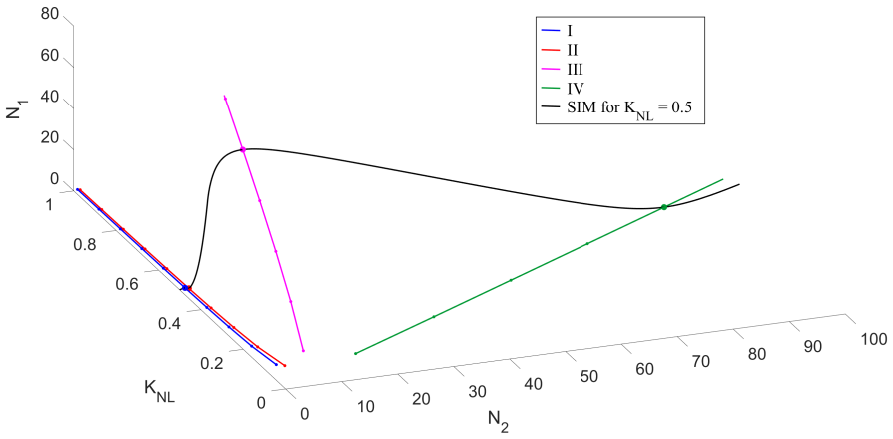

(a)

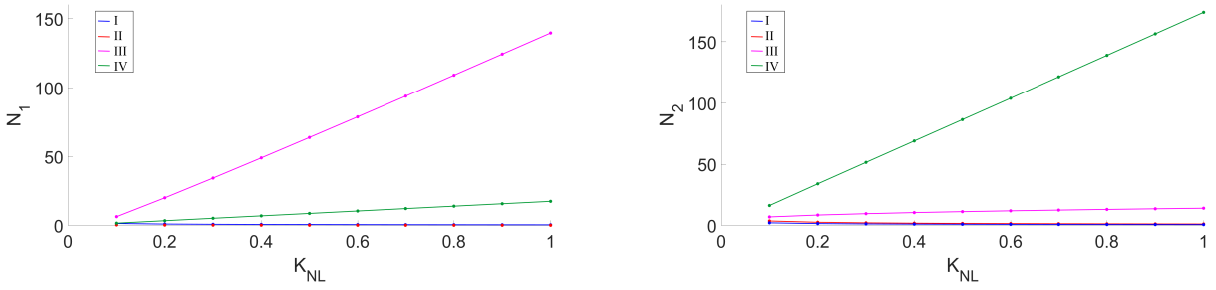

(b) (c)

Figure 9: a) Amplitudes of singular points with respect to the parameter K_{NL} of restoring forcing function. The black solid line represents the SIM of the system for $K_{NL} = 0.5$ and the two other parameters of Table 2; b) N_1 versus K_{NL}; c) N_2 versus K_{NL}.

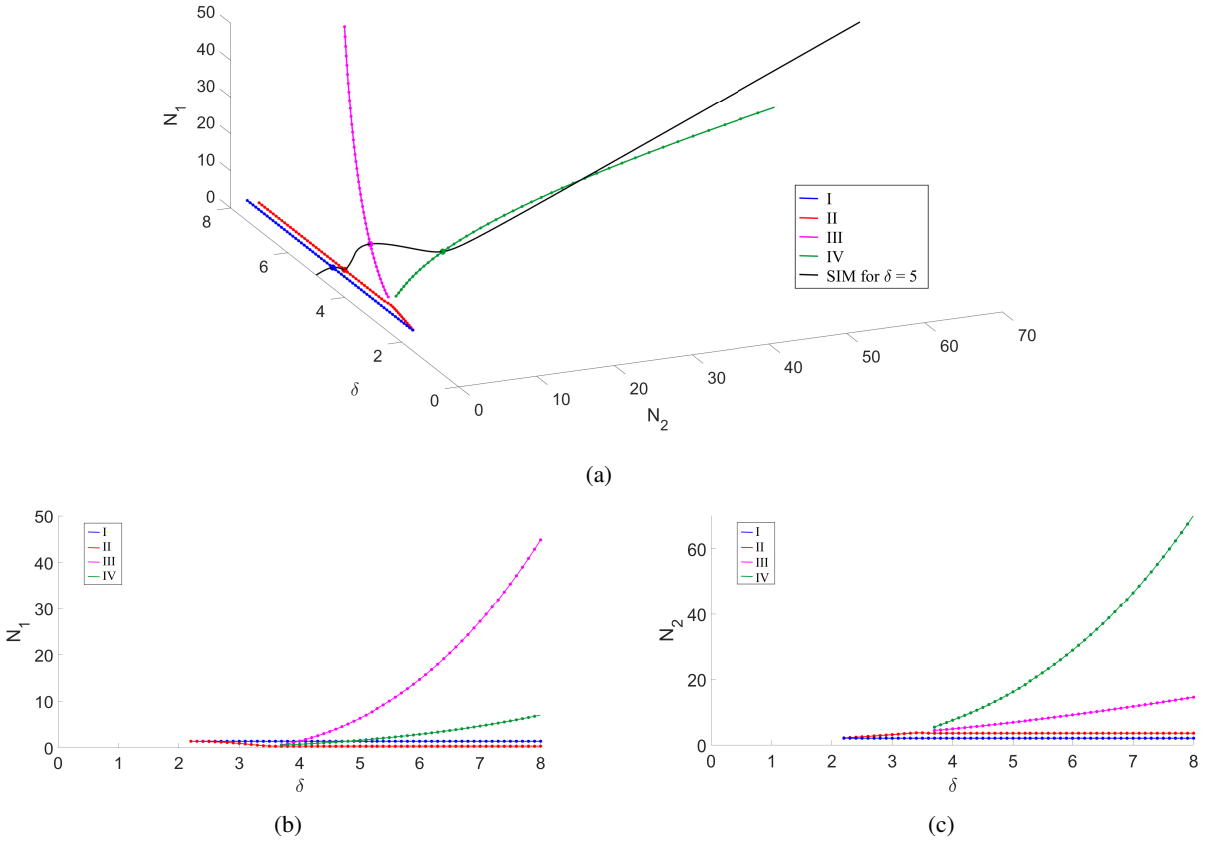

Figure 10: a) Amplitudes of singular points with respect to the parameter δ of restoring forcing function. The black solid line represents the SIM of the system for $\delta = 5$ and the two other parameters of Table 2; b) N_1 versus δ; c) N_2 versus δ.

sake of clarity, a SIM is plotted in the same figure for $\delta = 5$. Figures 10b and 10c present two-dimensional views of Fig. 10a. From this, it is observed the emergence of the singular lines III and IV from a minimum value of δ. Increasing this value, the amplitudes of these points increase significantly, mainly in terms of N_1 for III and in terms of N_2 for IV.

Let us summarize our observations from mentioned parametric studies here:

- The SIM can be tuned via modifying parameters of the restoring forcing function;
- These parameters affect mainly the singular lines III (second local maxima) and IV (second local minima) of the SIM;
- K_L affects mainly the singular line IV. Meanwhile, there is a value of K_L beyond which the singular lines III and IV disappear;
- K_{NL} influences the singular lines III and IV in a linear manner;
- δ influences the singular lines III and IV in a non-linear manner.

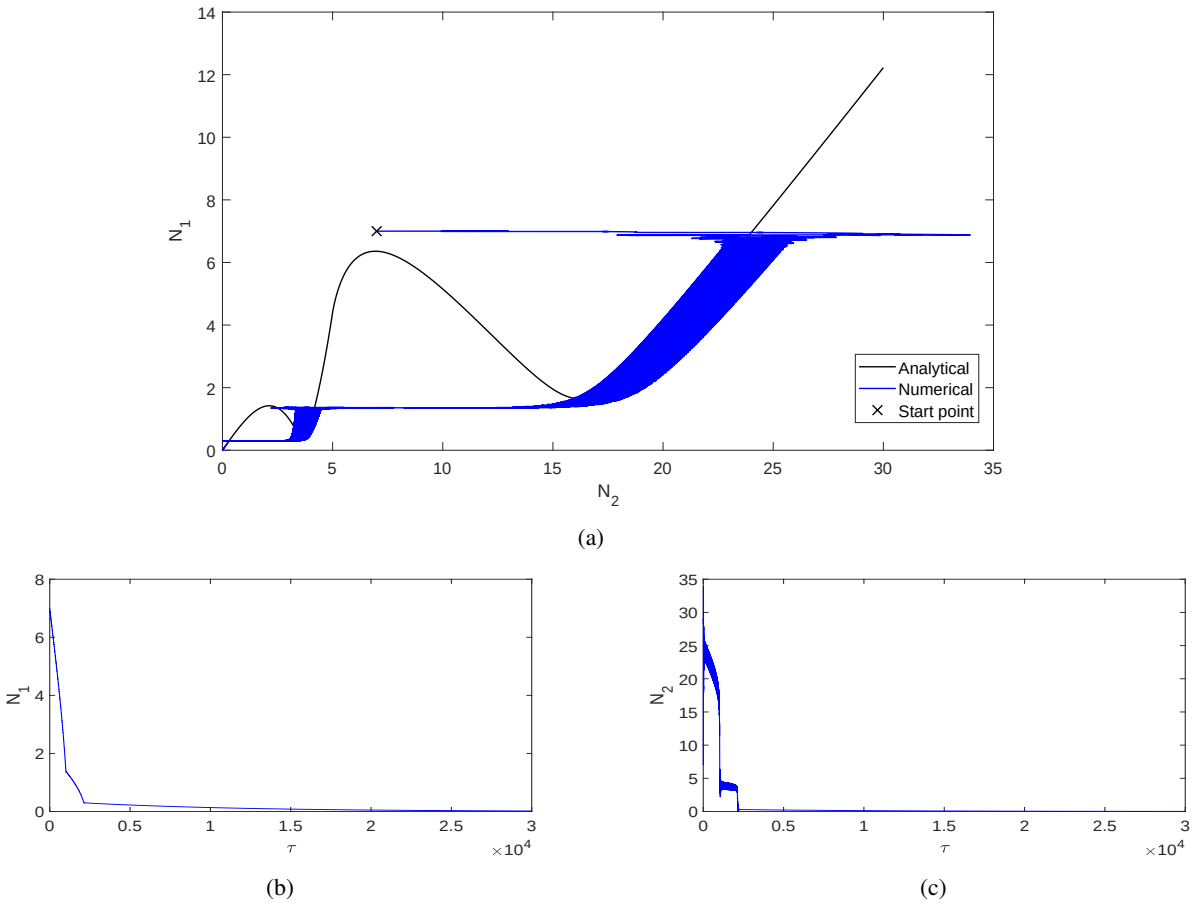

Figure 11: a) The SIM of the system and corresponding numerical results obtained by direct numerical integration of Eq. (7) with $\gamma = 0$ (free response). b) N_1 versus τ; c) N_2 versus τ. The initial conditions are $(w, v, \dot{w}, \dot{v}) = (7, 7, 0, 0)$.

5. Numerical examples

In this section, analytical developments of previous sections are compared with results obtained by numerical time integration of Eq. (7).

5.1. Meta-cell free response

Let us consider the following initial conditions: $(w, v, \dot{w}, \dot{v}) = (7, 7, 0, 0)$, illustrated by $\times$ symbol in Fig. 11a. Numerical results are added to the SIM of the system in Fig. 11a, while Figs. 11b and 11c summarize the time histories of system amplitudes. From Fig. 11a, it is seen that, starting from the initial condition $\times$, the system follows the SIM and, after double bifurcations due to the existence of two unstable zones of the SIM (see Fig. 4), the system reaches the rest position. The different geometry of the SIM, i.e., the possession of two unstable zones, compared to the one of systems with pure cubic nonlinearity, can permit more efficient energy exchanges in the meta-cell due to possible double bifurcations. Furthermore, as it can be seen in Figs. 11b and 11c, the vibratory energy reduction can be faster or slower depending on which branch of the SIM it occurs, i.e., depending on the energy levels.

For free responses, depending on initial conditions, the system can present two, one or no bifurcations. Let us consider the initial conditions $(w, v, \dot{w}, \dot{v}) = (2, 2, 0, 0)$ and $(w, v, \dot{w}, \dot{v}) = (1, 1, 0, 0)$, represented by $\times$ symbol in Figs. 12a and 12b, respectively. Numerical results of Fig. 12a present a simple bifurcation, while the results of Fig. 12b do not show any bifurcation due to the position of initial conditions, which are below the threshold of any bifurcation.

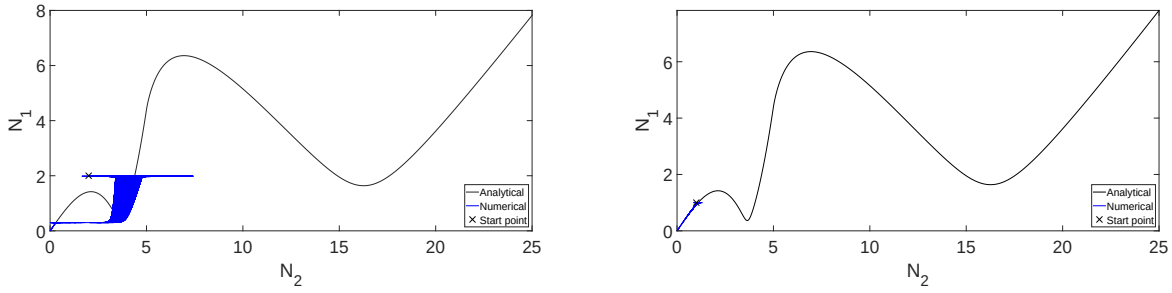

Figure 12: The SIM of the system and corresponding responses obtained by direct numerical integration of Eq. (7) with $\gamma = 0$. The initial conditions are: a) $(w, v, \dot{w}, \dot{v}) = (2, 2, 0, 0)$; b) $(w, v, \dot{w}, \dot{v}) = (1, 1, 0, 0)$.

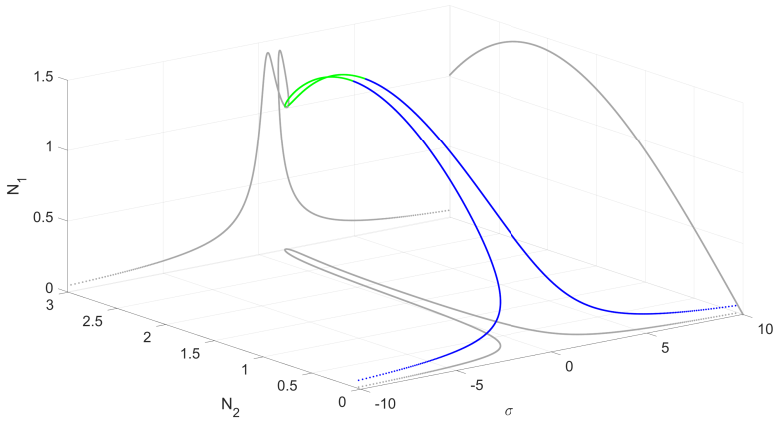

Figure 13: Branch of detected equilibrium points of the system with respect to the de-tuning parameter σ or deriving frequency ($\vartheta = 1 + \sigma\epsilon$) for the system with $\gamma = 1$. Projections of this three-dimensional curve on different plans are presented in grey. The unstable zone of the SIM is represented in green colour. Results are obtained from Eqs. (36) and (20).

5.2. Meta-cell forced responses

Here, we will present frequency response curves obtained from analytical developments (see Eq. (36)). Depending on the excitation amplitude γ, different frequency responses are observed, including the emergence of an isola. In addition, numerical results for some frequencies of excitation will be provided and compared with analytical predictions.

5.2.1. Meta-cell with external forcing amplitude $\gamma = 1$

A forced system with $\gamma = 1$ is studied. Equilibrium points of the system for sweeping de-tuning parameter σ or sweeping deriving frequency ($\vartheta = 1 + \sigma\epsilon$) are obtained from Eq. (36) and, then, from Eq. (20). The three-dimensional view of corresponding frequency responses of the system is illustrated in Fig. 13, as well as its orthogonal projections on each plane. In this figure, those equilibrium points situated in unstable zones of the SIM are highlighted. Two-dimensional views of Fig. 13 are presented in Figs. 14a and 14b. From these figures, it is seen that the system can present one, two or three equilibrium points according to the position of σ.

The two-dimensional view of Fig. 13 in terms of N_1 and N_2 is depicted in Fig. 14c. This figure is a part of the SIM of the system and it provides necessary information about positions of equilibrium points on the SIM for the given forcing amplitude and an interval of deriving frequency. In other words, Fig. 14c shows the geometrical positions of all possible equilibrium points on the SIM for $\gamma = 1$ and a given interval of σ. For the sake of clarity, the covered equilibrium points on the SIM for $\gamma = 1$ are framed in Fig. 14d. As a summary, analytical developments permit us to:

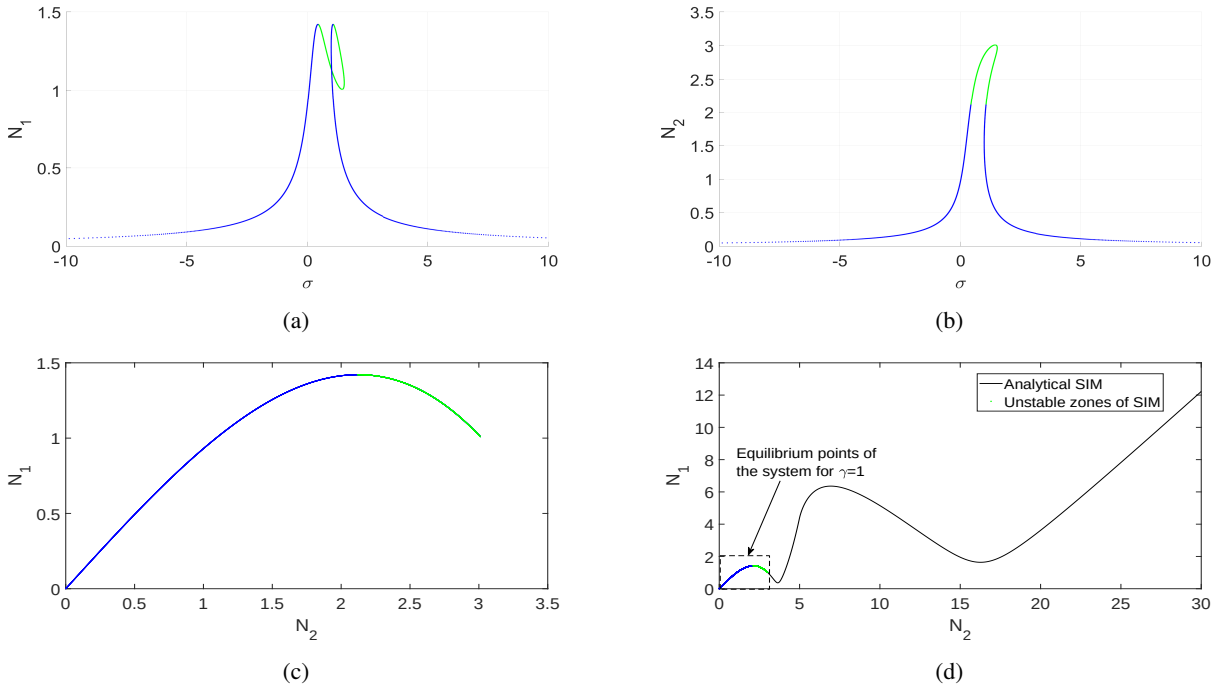

Figure 14: Two-dimensional views of Fig. 13. a) N_1 with respect to the de-tuning parameter σ; b) N_2 with respect to σ; c) N_1 versus N_2; d) Superposition of Fig. 14c on the SIM of Fig. 3.

- Identify three-dimensional frequency response curves;
- Detect the position of equilibrium points on the SIM for a given forcing amplitude and a sweeping frequency;
- Identify equilibrium points situated in the unstable zones of the SIM. If the system possess only one equilibrium point and it is situated in the unstable zone, it will present modulated response [46, 47];
- Identify all possible branches of frequency response curves, even the isola, which can correspond to high amplitude levels of the cell. This should be avoided if the objective is the system control, but it can be interesting if the objective is energy harvesting.

Let us consider some detuning parameters for the case of $\gamma = 1$ and compare analytical predictions with numerical results.

Meta-cell behaviour for $\sigma = 0$. For $\sigma = 0$, there is only one equilibrium point which is stable (Figs. 14a and 14b). A periodic response is thus expected whatever the initial conditions.
The SIM is plotted in Fig. 15a, as well as the corresponding numerical results for $\gamma = 1$, $\sigma = 0$ and the initial conditions $(w, v, \dot{w}, \dot{v}) = (0, 0, 0, 0)$. The behaviour of N_1 and N_2 over time can be visualized in Figs. 15b and 15c respectively, from which it is noticed that N_1 and N_2 present a periodic response, converging to the values of Figs. 14a and 14b, respectively, for $\sigma = 0$.

Meta-cell behaviour for $\sigma = 0.8$. From Figs. 14a and 14b, it is noticed the only equilibrium point for $\sigma = 0.8$ is situated in an unstable zone of the SIM. Thus, a modulated response [46] is expected whatever the initial conditions. It should be mentioned that this modulated response will be around the first pair of local extrema of the SIM (I and II in Fig. 4) because of the predictions depicted in Figs. 14c and 14d.
The SIM accompanied by numerical results for $\gamma = 1$, $\sigma = 0.8$ and the initial conditions $(w, v, \dot{w}, \dot{v}) = (0, 0, 0, 0)$ are presented in Fig. 16a. The behaviour of N_1 and N_2 over time can be visualized in Figs. 16b and 16c respectively, from which it is noticed that N_1 and N_2 present a modulated response, as predicted. These results show that the modulated response is around local extrema I and II as already predicted by analytical developments.

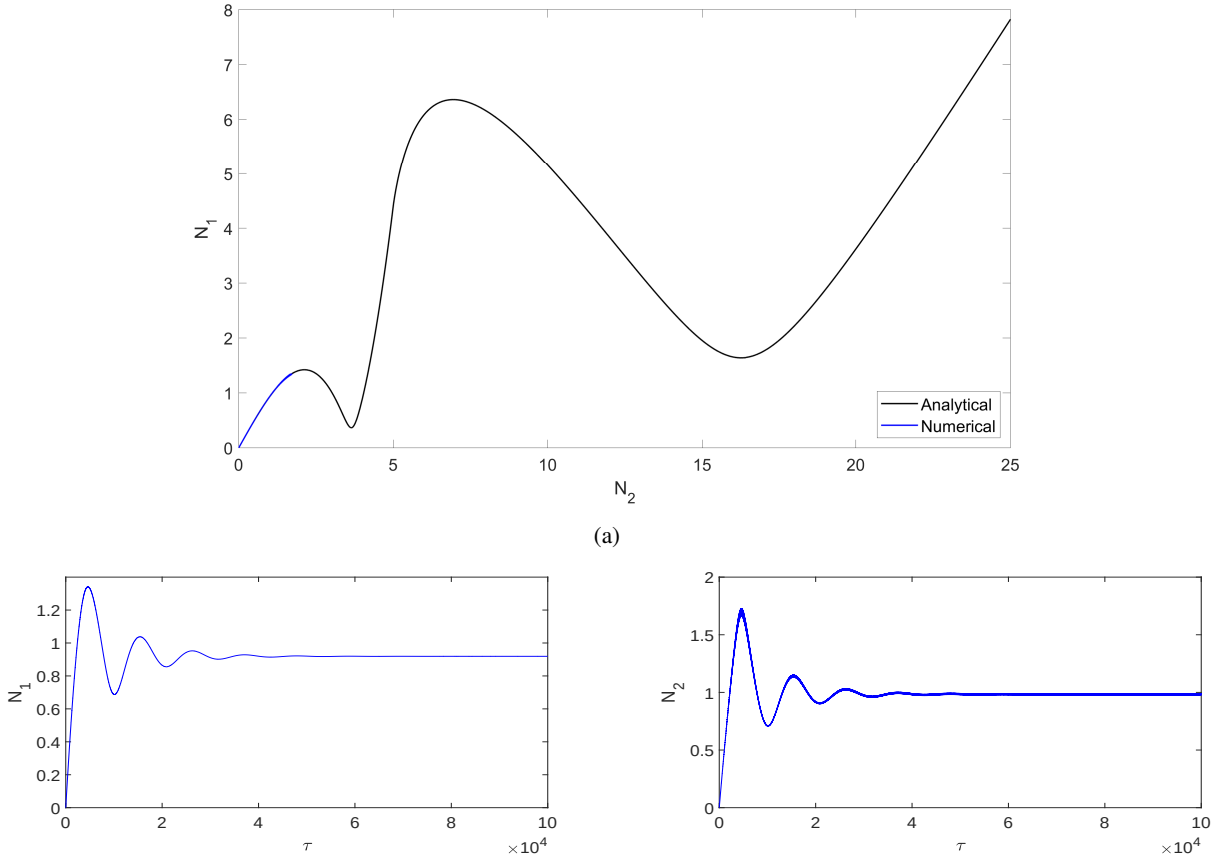

Figure 15: a) SIM of the system and corresponding numerical results obtained by direct numerical integration of Eq. (7). b) N_1 versus τ; c) N_2 versus τ. The system is under external excitation with $\gamma = 1$, $\sigma = 0$ and the initial conditions are $(w, v, \dot{w}, \dot{v}) = (0, 0, 0, 0)$.

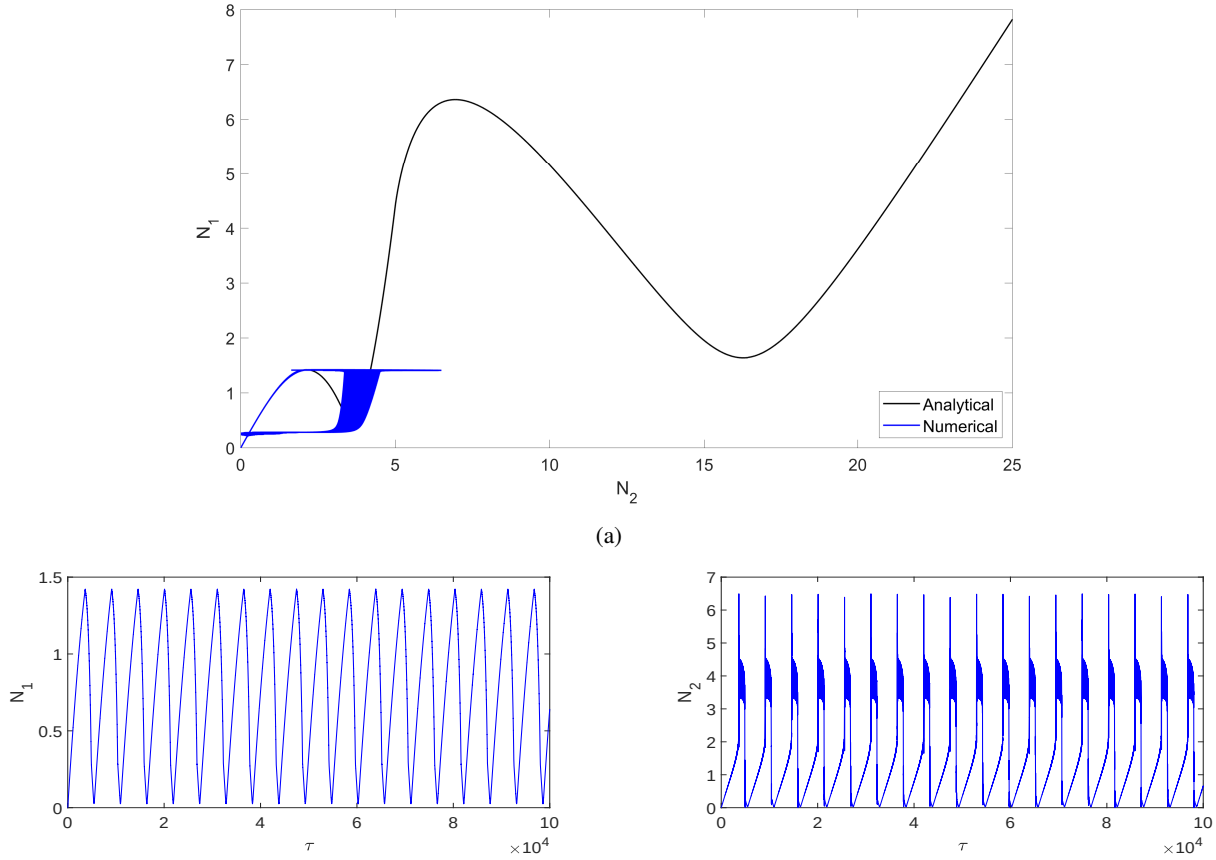

Figure 16: a) The SIM of the system and corresponding numerical results obtained by direct numerical integration of Eq. (7). b) N_1 versus τ; c) N_2 versus τ. The system is under external excitation with $\gamma = 1$, $\sigma = 0.8$ and the initial conditions are $(w, v, \dot{w}, \dot{v}) = (0, 0, 0, 0)$.

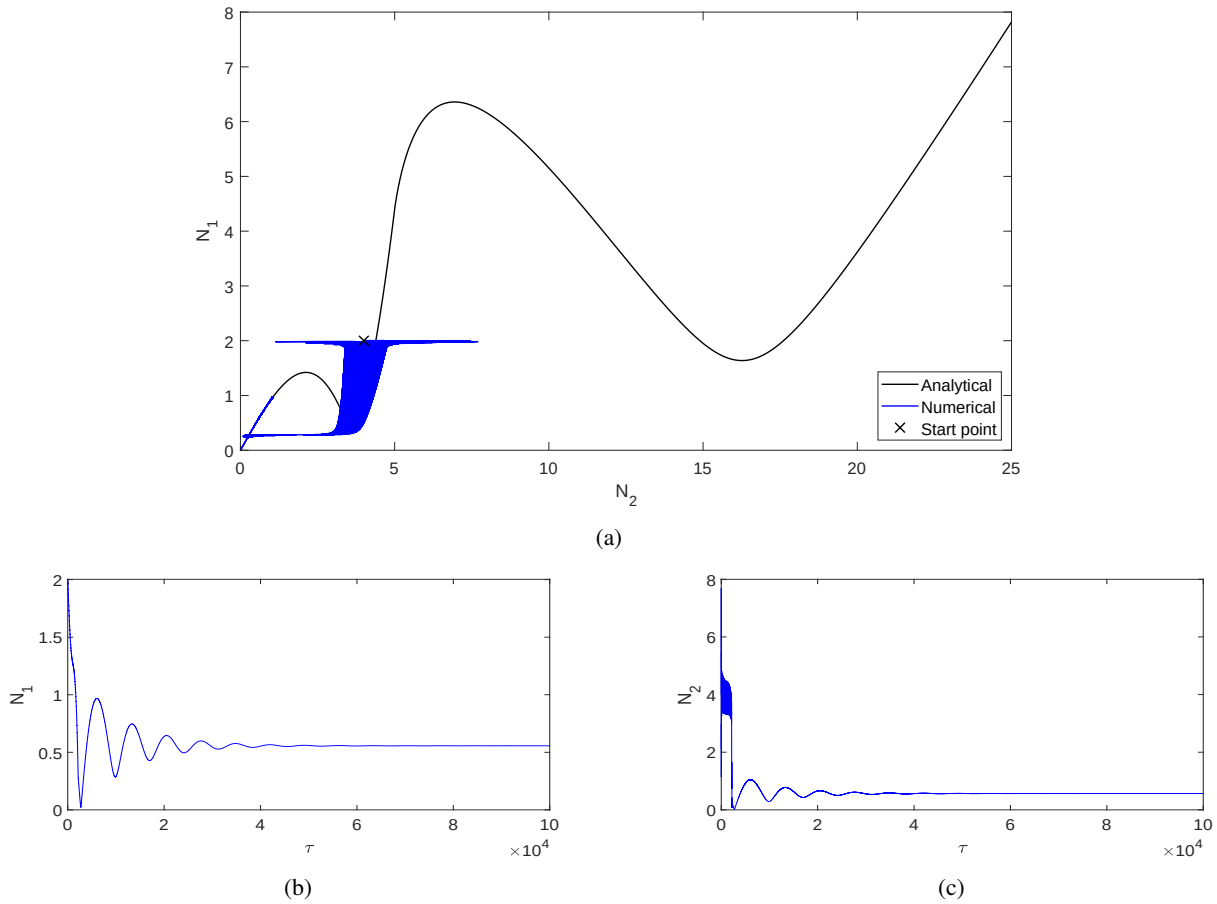

Figure 17: a) The SIM of the system and corresponding numerical results obtained by direct numerical integration of Eq. (7). b) N_1 versus τ; c) N_2 versus τ. The system is under external excitation with $\gamma = 1$, $\sigma = 1.4$ and the initial conditions are $(w, v, \dot{w}, \dot{v}) = (2, 4, 0, 0)$.

Meta-cell behaviour for $\sigma = 1.4$. For $\sigma = 1.4$, in Figs. 14a and 14b, there are three possible equilibrium points which two of them are in the unstable zone of the SIM. Thus, the system presents a periodic or possible modulated responses. The numerical results for $\gamma = 1$, $\sigma = 1.4$ and the initial conditions $(w, v, \dot{w}, \dot{v}) = (2, 4, 0, 0)$ are presented in Fig. 17, from which it is noticed that N_1 and N_2 present a periodic response.

5.2.2. *Meta-cell with external forcing amplitude* $\gamma = 2$

For a forcing amplitude γ bigger than than a certain value, the emergence of an isola is observed. This isola is represented in red colour in Fig. 18 for $\gamma = 2$. Two-dimensional views of Fig. 18 are presented in Figs. 19a and 19b. The isola could present high energy levels for the outer cell and be unsafe if the goal is the system control. However, for energy harvesting aspects, the isola could be interesting.

The two-dimensional view of Fig. 18 in terms of N_1 and N_2 is depicted in Fig. 19c and it is accompanied by the SIM in Fig. 19d, highlighting the position of the isola on the SIM for $\gamma = 2$. It is seen that the second main part of the SIM, corresponding to the second local maximum (i.e., point III in Fig. 4), is activated for this set of characteristics of external excitation. Let us now consider some detuning parameters for the case of $\gamma = 2$ and compare analytical predictions with numerical results.

Meta-cell behaviour for $\sigma = -1.8$. Figure 20a collects the SIM of the system and corresponding numerical results for $\gamma = 2$, $\sigma = -1.8$ and the initial conditions $(w, v, \dot{w}, \dot{v}) = (4, 4, 0, 0)$. The time histories of N_1 and N_2 can be visualized in Figs. 20b and 20c respectively. Comparing Figs. 19a and Fig. 20b, one can see that the system is attracted by the

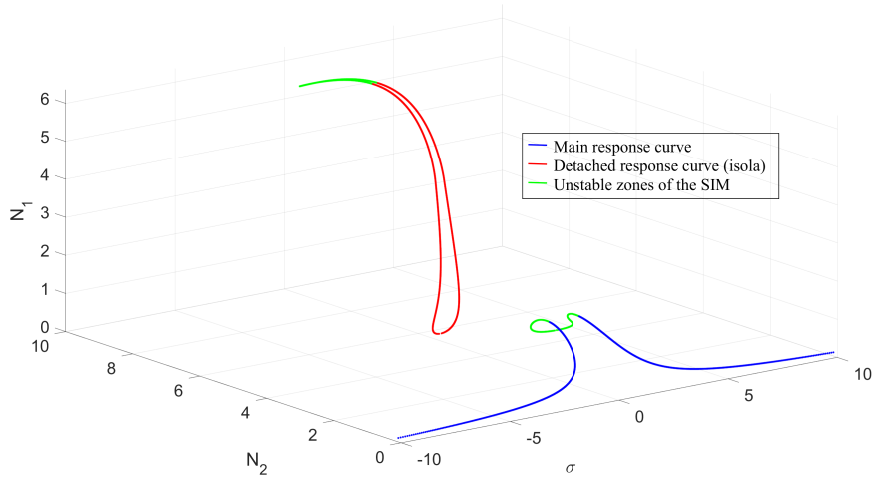

Figure 18: Detected equilibrium points of the system with respect to the de-tuning parameter σ or deriving frequency $(\vartheta = 1 + \sigma\epsilon)$ for the system with $\gamma = 2$. The unstable zone of the SIM is represented in green colour. Results are obtained from Eqs. (36) and (20).

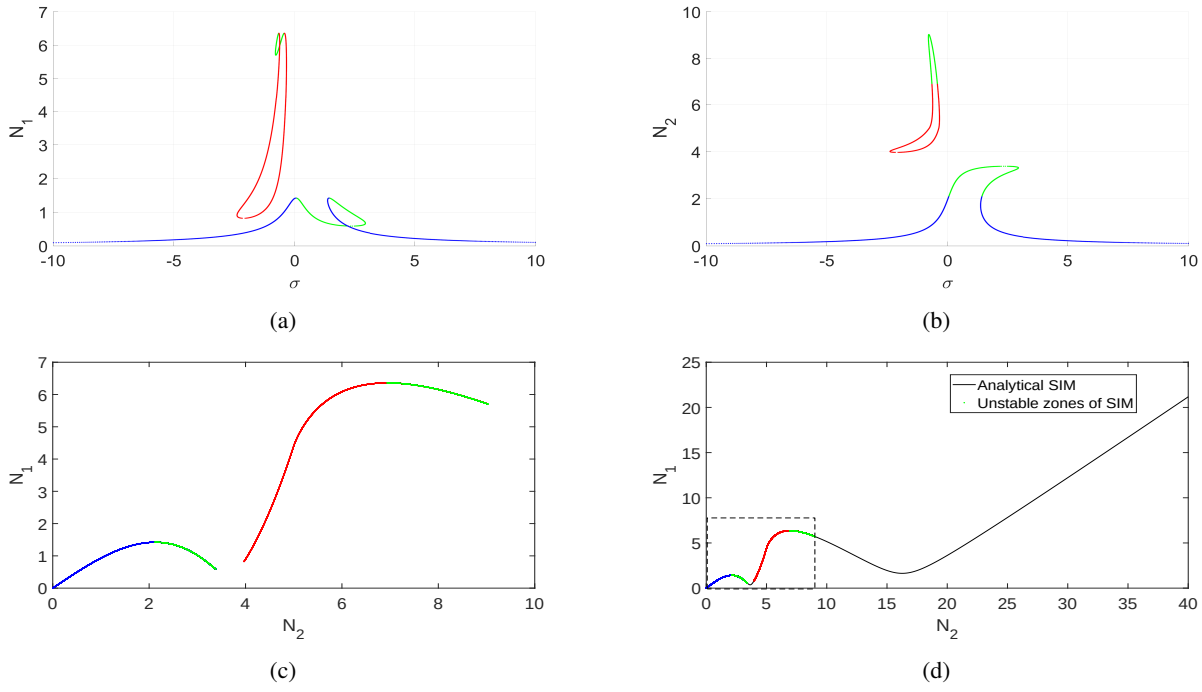

Figure 19: Two-dimensional views of Fig. 18. a) N_1 with respect to the de-tuning parameter σ; b) N_2 with respect to σ; c) N_1 versus N_2; d) Superposition of Fig. 19c on the SIM of Fig. 3.

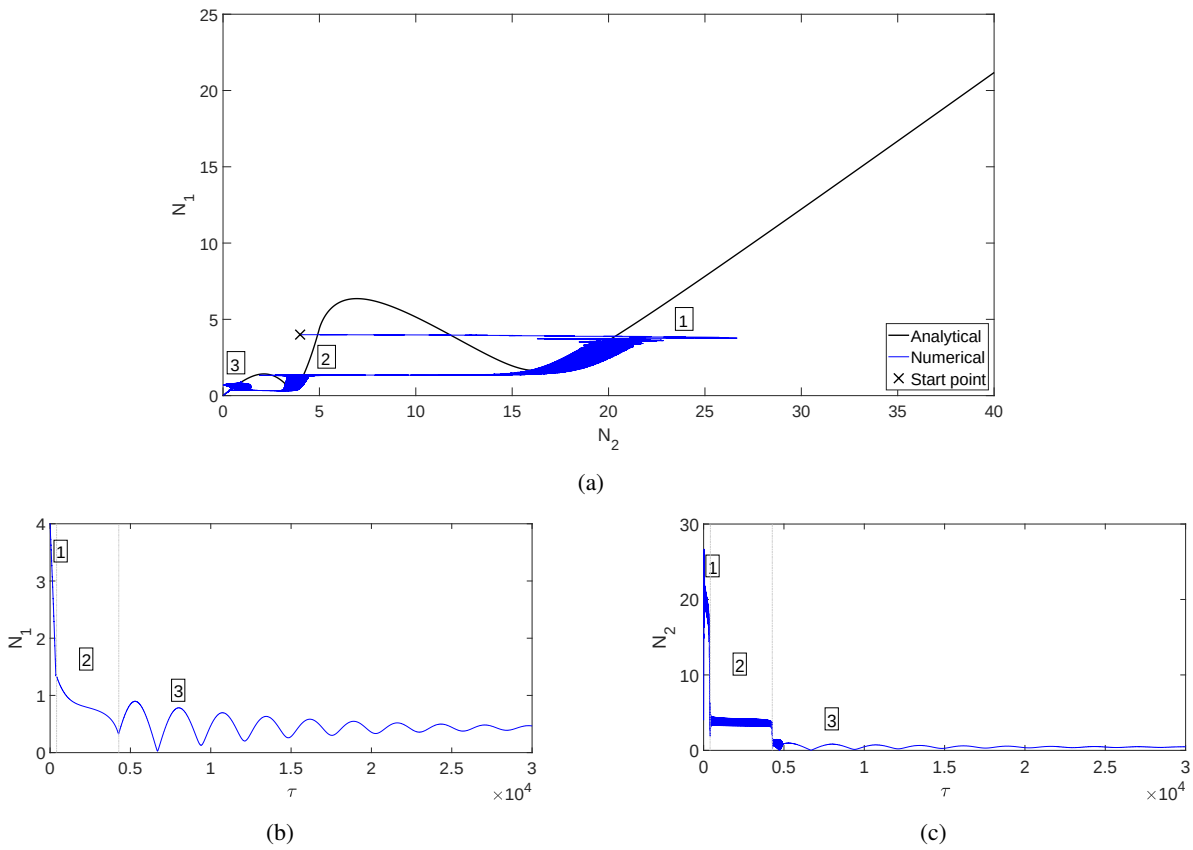

Figure 20: a) The SIM of the system and corresponding numerical results obtained by direct numerical integration of Eq. (7). b) N_1 versus τ; c) N_2 versus τ. Three phases of vibratory energy reduction are depicted in these figures. The system is under external excitation with $\gamma = 2$, $\sigma = -1.8$ and the initial conditions are $(w, v, \dot{w}, \dot{v}) = (4, 4, 0, 0)$.

lowest branch of frequency response curves for $\sigma = -1.8$.

Besides that, in Fig. 20, we spot three phases of energy reduction, namely: Phase 1 - very quickly; Phase 2 - less quickly; Phase 3 - slowly. This allows to have an absorber acting in different phases, which can be adjusted with the proper design of the SIM. Depending on the initial conditions, the system may reaches a higher equilibrium point located in the isola. This behaviour can be observed for the initial conditions $(w, v, \dot{w}, \dot{v}) = (14, 7, 0, 0)$ in Fig. 21a. This can be spotted via comparing the results of numerical integration (Figs. 21b and 21c) and the values of N_1 and N_2 in Figs. 19a and 19b, respectively, for $\sigma = -1.8$.

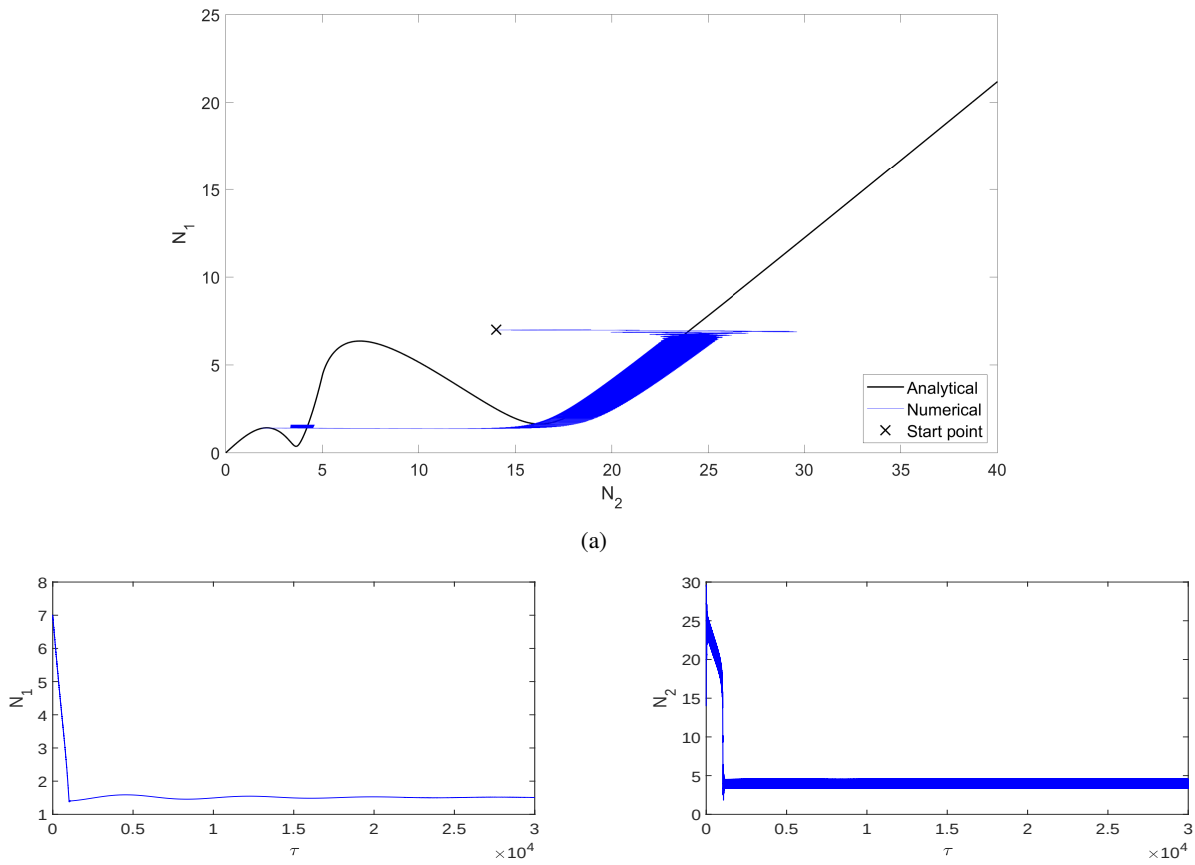

Figure 21: a) The SIM of the system and corresponding numerical results obtained by direct numerical integration of Eq. (7). b) N_1 versus τ; c) N_2 versus τ. The system is under external excitation with $\gamma = 2$, $\sigma = -1.8$ and the initial conditions are $(w, v, \dot{w}, \dot{v}) = (14, 7, 0, 0)$.

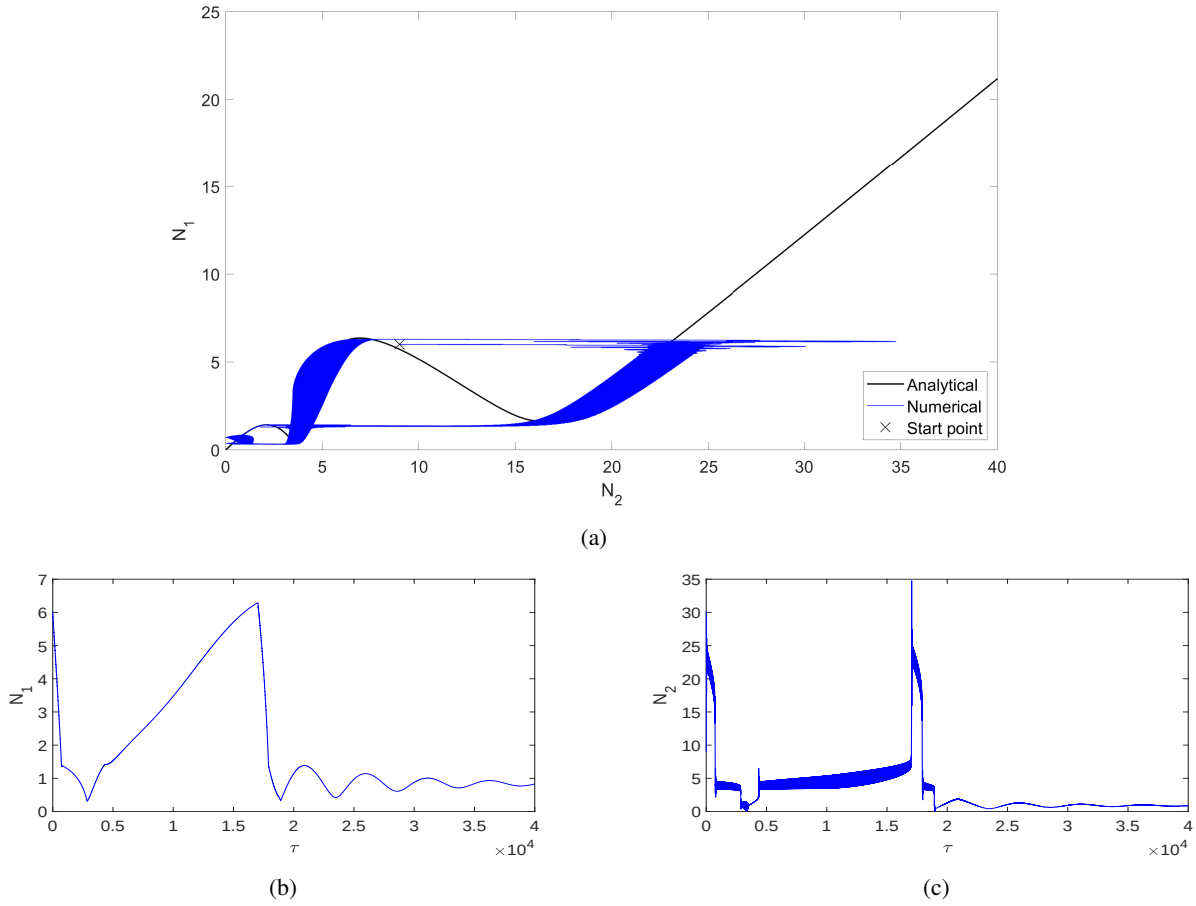

Figure 22: a) The SIM of the system and corresponding numerical results obtained by direct numerical integration of Eq. (7). b) N_1 versus τ; c) N_2 versus τ. The system is under external excitation with $\gamma = 2$, $\sigma = -0.66$ and the initial conditions are $(w, v, \dot{w}, \dot{v}) = (6, 9, 0, 0)$.

Meta-cell behaviour for $\sigma = -0.66$. The SIM is plotted in Fig. 22a, accompanied by numerical results for $\gamma = 2$, $\sigma = -0.66$ with initial conditions $(w, v, \dot{w}, \dot{v}) = (6, 9, 0, 0)$. The behaviour of N_1 and N_2 over time can be visualized in Figs. 22b and 22c respectively. In this case, it is observed that after double bifurcations the system reaches a periodic regime situated on the lowest branch of the frequency response curves.

Meta-cell behaviour for $\sigma = 1$. For $\sigma = 1$ in Figs. 19a and 19b, it is seen that the equilibrium point is situated in an unstable zone of the SIM. The SIM is plotted in Fig. 23a, as well as the numerical results for the initial conditions $(w, v, \dot{w}, \dot{v}) = (0, 0, 0, 0)$. Time histories of N_1 and N_2 are presented in Figs. 23b and 23c respectively. From these figures, it is observed that the system reaches a modulated regime as predicted by analytical developments.

5.2.3. Meta-cell with external forcing amplitude $\gamma = 10$

Equilibrium points of the system for sweeping de-tuning parameter σ are collected in Fig. 24 for $\gamma = 10$. Different two-dimensional views of Fig. 24 are presented in Fig. 25. This figure shows that the forcing amplitude $\gamma = 10$ activates both zones of local extrema of the SIM.

As a summary, the analytical developments in this paper permit predicting equilibrium points of the system without ignoring possible isola.

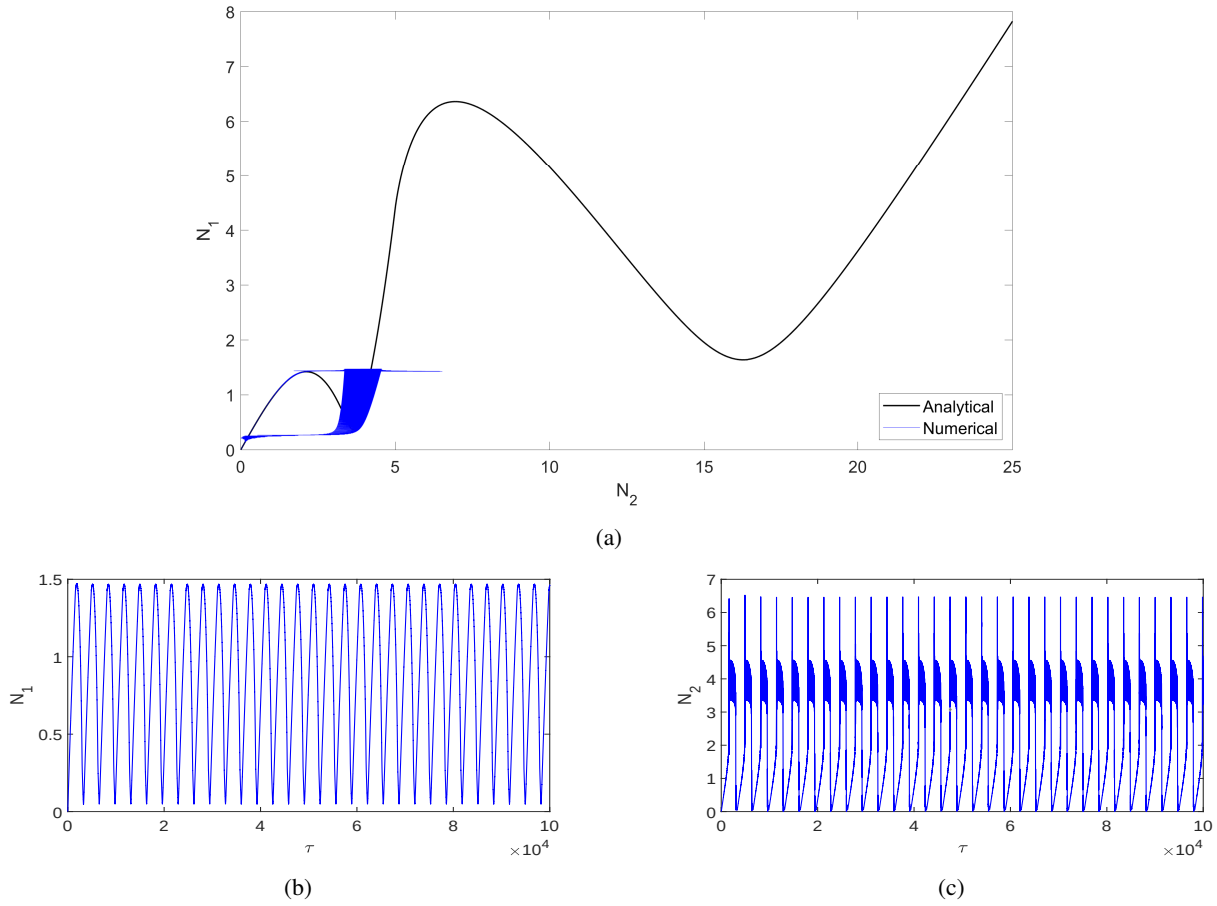

Figure 23: a) The SIM of the system and corresponding numerical results obtained by direct numerical integration of Eq. 7. b) N_1 versus τ; c) N_2 versus τ. The system is under external excitation with $\gamma = 2$, $\sigma = 1$ and the initial conditions are $(w, v, \dot{w}, \dot{v}) = (0, 0, 0, 0)$.

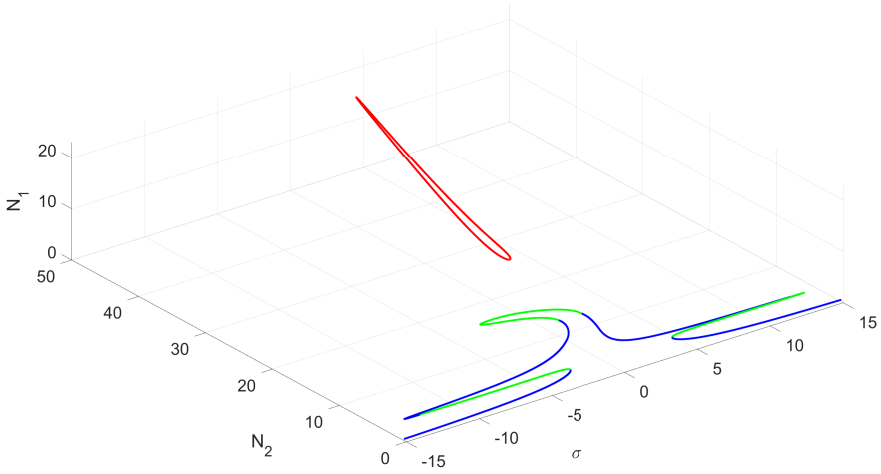

Figure 24: Detected equilibrium points of the system with respect to the de-tuning parameter σ or deriving frequency $(\vartheta = 1 + \sigma\epsilon)$ for $\gamma = 10$. The unstable zone of the SIM is represented in green colour. Results are obtained from Eqs. (36) and (20).

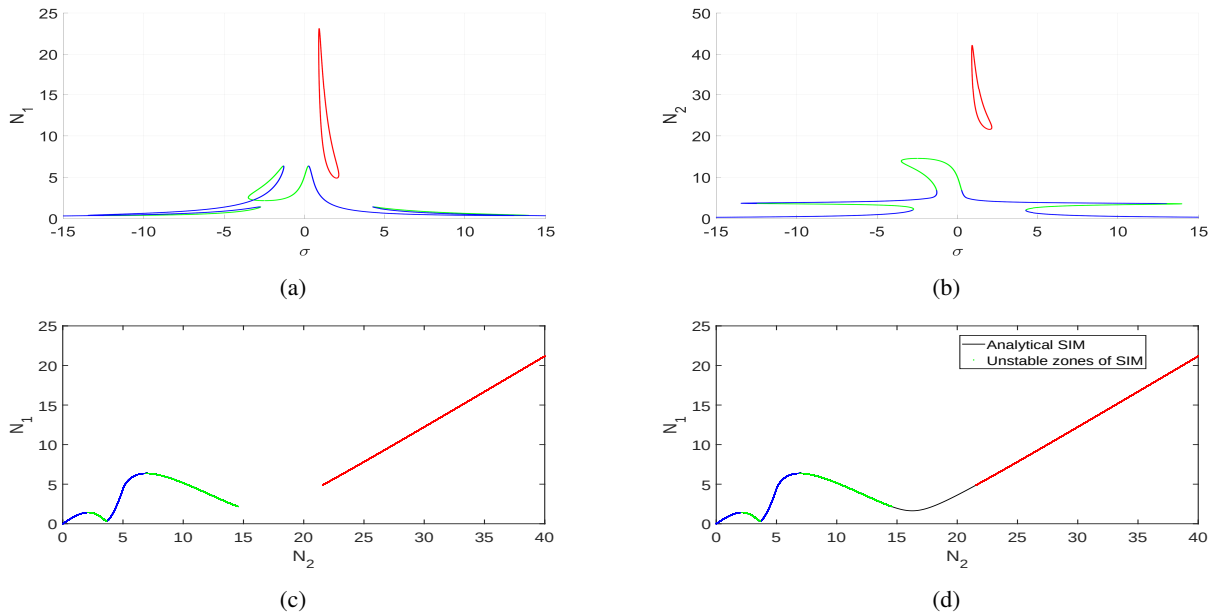

Figure 25: Two-dimensional views of Fig. 24. a) N_1 with respect to the de-tuning parameter σ; b) N_2 with respect to σ; c) N_1 versus N_2; d) Superposition of Fig. 25c on the SIM of Fig. 3.

5.3. Backbone curves

The backbone curves provide an overall vision of all possible dynamical behaviours of the system, as we can see in Fig. 26, where the frequency response curves corresponding to different values of γ treated in Sect. 5.2 are added to Fig. 5. The Fig. 26 shows the emergence of possible non-continuous frequency responses of the system with an isola placed in the B2 or B3 branches. Moreover, it is seen that the backbone curves pass (almost) through local extrema of frequency responses under different external forcing amplitudes.

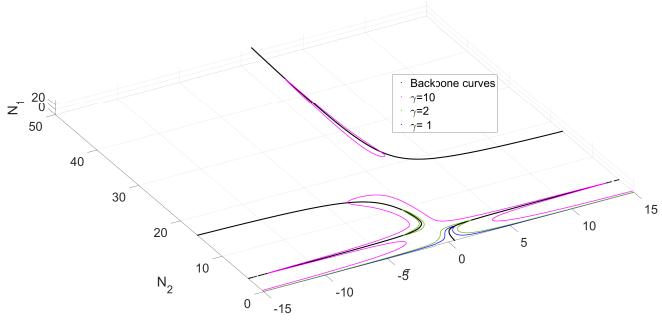

Figure 26: Backbone and frequency response curves for different values of γ.

6. Conclusions

Vibratory energy exchanges between particles of a two degree of freedom system are studied. The system can be considered as a meta-cell that is composed of an outer mass which houses an inner mass with a compound nonlinearity. Fast and slow dynamics of the system were investigated, leading to detection of the slow invariant manifold and also of dynamical characteristic points. The compound nonlinearity of the inner mass results in a slow invariant manifold with four local extrema, differing from corresponding ones of systems with pure cubic and piecewise-linear nonlinearities. The frequency response curves, with a three-dimensional view of detected equilibrium points, permit identifying possible isola and the position of equilibrium points on the slow invariant manifold, especially in its unstable zones. Depending on the nature of the equilibrium points and on the existence of singularities, the system can present one, two or several bifurcations, leading to final periodic or non-periodic regimes. Furthermore, the vibratory energy reduction can be faster or slower depending on which branch of the slow invariant manifold it occurs, i.e., depending on the energy levels. This allows to have an absorber acting in different phases, which can be adjusted with the proper design of the slow invariant manifold.

Special attention must be paid to systems which present isola. If the objective is the system control, these isola should not present high energy levels for the cell. However, these isola can be interesting for energy harvesting aspects. The analytical developments in this paper provide design tools for tuning the compound nonlinearity of the inner mass for imposed objectives (control or energy harvesting). Moreover, we can design the inner mass in a manner that the system presents special types of responses, i.e., periodic or non-periodic, for given external forcing characteristics. The considered system can be used for the control process of the outer mass by a nonlinear energy sink with compound nonlinearity or be considered as a single meta-cell with spacial characteristics in a chain of nonlinear mass-in-mass systems. The outlook of this paper will be the experimentation of such single meta-cell and then the study of it in the form of a chain.

Acknowledgments

This work was supported by the LABEX CeLyA (ANR-10-LABX-0060) of Université de Lyon, within the program "Investissements d'Avenir" operated by the French National Research Agency (ANR).

References

[1] H. Frahm, Device for damping vibrations of bodies, uS Patent 989,958 (Apr. 18 1911).
[2] J. P. D. Hartog, Mechanical vibrations, McGraw-Hill, New York, N.Y., 1947.
[3] R. E. Roberson, Synthesis of a nonlinear dynamic vibration absorber, Journal of Franklin Institute 254 (1952) 205–220.
[4] R. F. Henry, S. A. Tobias, Instability and steady-state coupled motions in vibration isolating suspensions, Journal of Mechanical Engineering Science 1 (1959) 19–29.
[5] R. F. Henry, S. A. Tobias, Modes at rest and their stability in coupled non-linear systems, Journal of Mechanical Engineering Science 3 (1961) 163–173.
[6] E. Sevin, On the parametric excitation of pendulum-type vibration absorber, Journal of Applied Mechanics 28 (1961) 330–334.
[7] R. A. Struble, J. H. Heinbockel, Resonant oscillations of a beam-pendulum system, Journal of Applied Mechanics 30 (1963) 181–188.
[8] R. S. Haxton, A. D. S. Barr, The autoparametric vibration absorber, Journal of Engineering for Industry 94 (1972) 119–125.
[9] I. Yamakawa, S. Takeda, H. Kojima, Behavior of a new type dynamic vibration absorber, Bulletin of JSME 20 (146) (1977) 947–954.
[10] H. Kojima, H. Saito, Forced vibration of a beam with a non-linear dynamic absorber, Journal of Sound and Vibration 88 (4) (1983) 559–568.
[11] J. B. Hunt, J.-C. Nissen, The broadband dynamic vibration absorber, Journal of Sound and Vibration 83 (4) (1982) 573–578.
[12] J.-C. Nissen, K. Popp, B. Schmalhorst, Optimization of a non-linear dynamic vibration absorber, Journal of Sound and Vibration 99 (1) (1985) 149–154.
[13] H. J. Rice, J. R. McCraith, Practical non-linear vibration absrober design, Journal of Sound and Vibration 116 (3) (1987) 545–559.
[14] S. Ema, E. Marui, Damping characteristics of an impact damper and its application, International Journal of Machine Tools and Manufacture 36 (3) (1996) 293–306.
[15] S. Ema, E. Marui, Suppression of chatter vibration of boring tools using impact dampers, International Journal of Machine Tools and Manufacture 4 (2000) 1141–1156.
[16] O. Gendelman, L. Manevitch, A. Vakakis, R. M'Closkey, Energy pumping in nonlinear mechanical oscillators: Part I-dynamics of the underlying hamiltonian systems, Journal of Applied Mechanics-transactions of The Asme 68 (2001) 34–41. doi:10.1115/1.1345524.
[17] A. Vakakis, Inducing passive nonlinear energy sinks in vibrating systems, Journal of Vibration and Acoustics 123 (2001) 42–48. doi:10.1115/1.1368883.
[18] A. Vakakis, O. Gendelman, Energy pumping in nonlinear mechanical oscillators: Part II-resonance capture, Journal of Applied Mechanics-transactions of The Asme 68. doi:10.1115/1.1345525.

[19] F. Nucera, A. Vakakis, D. McFarland, L. Bergman, G. Kerschen, Targeted energy transfers in vibro-impact oscillators for seismic mitigation, Nonlinear Dynamics 50 (3) (2007) 651–677.
[20] O. Gendelman, Analytic treatment of a system with a vibro-impact nonlinear energy sink, Journal of Sound and Vibration 331 (2012) 45994608.
[21] E. Gourc, G. Michon, S. Seguy, A. Berlioz, Targeted energy transfer under harmonic forcing with a vibro-impact nonlinear energy sink: Analytical and experimental developments, Journal of Vibration and Acoustics 137 (3).
[22] C.-H. Lamarque, O. Gendelman, A. Ture Savadkoohi, E. Etcheverria, Targeted energy transfer in mechanical systems by means of non-smooth nonlinear energy sink, Acta mechanica 221 (1) (2011) 175–200.
[23] M. Weiss, B. Vaurigaud, A. Ture Savadkoohi, C.-H. Lamarque, Control of vertical oscillations of a cable by a piecewise linear absorber, Journal of Sound and Vibration 435 (2018) 281–300.
[24] G. Hurel, A. Ture Savadkoohi, C.-H. Lamarque, Design of a nonlinear absorber for a 2 degrees of freedom pendulum and experimental validation, Structural Control and Health Monitoring 28 (11) (2021) e2814. doi:https://doi.org/10.1002/stc.2814.
[25] A. Ture Savadkoohi, C.-H. Lamarque, M. Contessa, Trapping vibratory energy of main linear structures by coupling light systems with geometrical and material non-linearities, International Journal of Non-Linear Mechanics 80 (2016) 3–13.
[26] Y. S. Lee, A. F. Vakakis, L. A. Bergman, D. M. McFarland, G. Kerschen, Suppression aeroelastic instability using broadband passive targeted energy transfers, part I: Theory, AIAA journal 45 (3) (2007) 693–711.
[27] Y. S. Lee, G. Kerschen, D. M. McFarland, W. J. Hill, C. Nichkawde, T. W. Strganac, L. A. Bergman, A. F. Vakakis, Suppressing aeroelastic instability using broadband passive targeted energy transfers, part II: experiments, AIAA journal 45 (10) (2007) 2391–2400.
[28] O. Gendelman, A. Vakakis, L. Bergman, D. McFarland, Asymptotic analysis of passive nonlinear suppression of aeroelastic instabilities of a rigid wing in subsonic flow, SIAM Journal on Applied Mathematics 70 (5) (2010) 1655–1677.
[29] B. Vaurigaud, L. Manevitch, C.-H. Lamarque, Passive control of aeroelastic instability in a long span bridge model prone to coupled flutter using targeted energy transfer, Journal of Sound and Vibration 330 (11) (2011) 2580–2595.
[30] A. Luongo, D. Zulli, Aeroelastic instability analysis of NES-controlled systems via a mixed multiple scale/harmonic balance method, Journal of Vibration and Control 20 (13) (2014) 1985–1998.
[31] E. Gourdon, N. Alexander, C. Taylor, C.-H. Lamarque, S. Pernot, Nonlinear energy pumping under transient forcing with strongly nonlinear coupling: Theoretical and experimental results, Journal of Sound and Vibration 300 (3) (2007) 522–551.
[32] A. Ture Savadkoohi, B. Vaurigaud, C.-H. Lamarque, S. Pernot, Targeted energy transfer with parallel nonlinear energy sinks, part II: theory and experiments, Nonlinear Dynamics 67 (1) (2012) 37–46.
[33] N. Wierschem, S. Hubbard, J. Luo, L. Fahnestock, B. Spencer, D. McFarland, D. Quinn, A. Vakakis, L. Bergman, Response attenuation in a large-scale structure subjected to blast excitation utilizing a system of essentially nonlinear vibration absorbers, Journal of Sound and Vibration 389 (2017) 52–72.
[34] B. Cochelin, P. Herzog, P.-O. Mattei, Experimental evidence of energy pumping in acoustics, Comptes Rendus Mécanique 334 (11) (2006) 639–644.
[35] R. Bellet, B. Cochelin, P. Herzog, P.-O. Mattei, Experimental study of targeted energy transfer from an acoustic system to a nonlinear membrane absorber, Journal of Sound and Vibration 329 (14) (2010) 2768–2791.
[36] H. Huang, C. Sun, G. Huang, On the negative effective mass density in acoustic metamaterials, International Journal of Engineering Science 47 (4) (2009) 610–617. doi:10.1016/j.ijengsci.2008.12.007.
[37] L. I. Manevitch, The Description of Localized Normal Modes in a Chain of Nonlinear Coupled Oscillators Using Complex Variables, Nonlinear Dynamics 25 (1) (2001) 95–109. doi:10.1023/A:1012994430793.
[38] Federal Research Center for Chemical Physics, Russia Academy of Science, V. Smirnov, L. Manevitch, Federal Research Center for Chemical Physics, Russia Academy of Science, Complex Envelope Variable Approximation in Nonlinear Dynamics, Nelineinaya Dinamika 16 (3) (2020) 491–515. doi:10.20537/nd200307.
[39] A. H. Nayfeh, D. T. Mook, Nonlinear oscillations, wiley classics library ed Edition, Wiley classics library, Wiley, New York, 1995, oCLC: 257285431.
[40] A. Ture Savadkoohi, C.-H. Lamarque, M. Weiss, B. Vaurigaud, S. Charlemagne, Analysis of the 1:1 resonant energy exchanges between coupled oscillators with rheologies, Nonlinear Dynamics 86 (4) (2016) 2145–2159. doi:10.1007/s11071-016-2792-3.
[41] S. Charlemagne, A. Ture Savadkoohi, C.-H. Lamarque, Interactions Between Two Coupled Nonlinear Forced Systems: Fast/Slow Dynamics, International Journal of Bifurcation and Chaos 26 (09) (2016) 1650155. doi:10.1142/S0218127416501558.
[42] H. Guo, T. Yang, Y. Chen, L.-Q. Chen, Singularity analysis on vibration reduction of a nonlinear energy sink system, Mechanical Systems and Signal Processing 173 (2022) 109074. doi:10.1016/j.ymssp.2022.109074.
URL https://linkinghub.elsevier.com/retrieve/pii/S088832702200245X
[43] O. V. Gendelman, Targeted energy transfer in systems with non-polynomial nonlinearity, Journal of Sound and Vibration 315 (3) (2008) 732–745. doi:10.1016/j.jsv.2007.12.024.
[44] O. V. Gendelman, Y. Starosvetsky, M. Feldman, Attractors of harmonically forced linear oscillator with attached nonlinear energy sink I: Description of response regimes, Nonlinear Dynamics 51 (1-2) (2007) 31–46. doi:10.1007/s11071-006-9167-0.
[45] O. V. Gendelman, Targeted energy transfer in systems with non-polynomial nonlinearity, Journal of Sound and Vibration 315 (3) (2008) 732–745, eUROMECH colloquium 483, Geometrically non-linear vibrations of structures. doi:https://doi.org/10.1016/j.jsv.2007.12.024.
URL https://www.sciencedirect.com/science/article/pii/S0022460X07009947
[46] Y. Starosvetsky, O. Gendelman, Strongly modulated response in forced 2DOF oscillatory system with essential mass and potential asymmetry, Physica D: Nonlinear Phenomena 237 (13) (2008) 1719–1733. doi:10.1016/j.physd.2008.01.019.
[47] G. Hurel, A. Ture Savadkoohi, C.-H. Lamarque, Nonlinear Vibratory Energy Exchanges between a Two-Degree-of-Freedom Pendulum and a Nonlinear Absorber, Journal of Engineering Mechanics 145 (8) (2019) 04019058. doi:10.1061/(ASCE)EM.1943-7889.0001620.